# Off-resonant transient birefringence in liquids

Minhaeng Cho, Mei Du, Norbert F. Scherer,[a] and Graham R. Fleming
*Department of Chemistry and the James Franck Institute, The University of Chicago, Chicago, Illinois 60637*

Shaul Mukamel
*Department of Chemistry, University of Rochester, Rochester, New York 14627*

(Received 11 March 1993; accepted 30 April 1993)

Off-resonant transient birefringence measurements are analyzed using a reduced equation of motion for the ground state density matrix, which is expanded using an effective Hamiltonian. Assuming that the pump field is weak, we express the polarization relevant for the birefringence signal in terms of a convolution of the tensorial polarizability response function with the external fields. The homodyne-detected birefringence signal is directly compared with the coherent Raman signal. The relationship between off-resonant birefringence and spontaneous Raman experiments is discussed. By expanding the polarizability in powers of the nuclear coordinates and applying the Brownian oscillator model to the coordinate response function, we separate the birefringence signal into intra- and intermolecular coordinate response functions. Off-resonant transient birefringences of acetonitrile, chloroform, dimethylsulfoxide, and a series of alcohols were measured. The data are transformed to the frequency domain by using a model independent analysis method. The spectra are discussed in the context of various models for the distribution of intermolecular modes (spectral density) in liquids.

## I. INTRODUCTION

Ultrafast nuclear motions in liquids have been probed using a number of time-domain spectroscopies, such as the optical Kerr effect (OKE),[1–5] impulsive stimulated Raman scattering (ISRS),[6,7] and time-dependent fluorescence Stokes shift (TDFSS).[8–14] Although each measurement contains different information on the response of the material system with respect to an electric perturbation, these dynamical responses of the liquid should be understandable in terms of an underlying microscopic description of the liquid.

For example, electronically off-resonant measurements such as transient birefringence (i.e., optical Kerr effect) and femtosecond coherent Raman scattering (i.e., impulsive stimulated Raman scattering) are induced by an impulsive ($\delta$-function-like) electric perturbation, which results from a simple ultra-short pulse or two such pulses with different wave vectors, respectively. Thus the *pulse-response function* is relevant to the off-resonant transient birefringence and coherent Raman scattering signals. On the other hand, electronically resonant measurements such as the time-dependent fluorescence Stokes shift (TDFSS) technique reveal the liquid responses with respect to a step-like perturbation generated by a sudden change in the electronic charge distribution of the solute upon electronic excitation. Therefore, the TDFSS signal is related to the *step-response function* of the solvent. The pulse response and the step response functions are related to the imaginary [$G(t)$] and the real [$C(t)$] parts of the appropriate (one-sided) quantum mechanical correlation function, $\langle Q(0)Q(t)\rangle$.[15] Techniques such as hole burning show the evolution of both excited state particle and ground state hole and thus have two components which depend, respectively, on both types of response functions. It should be noted that, although the time-dependent properties of the perturbations induced by the field are different for off-resonant transient birefringence (and coherent Raman scattering) and the time-dependent fluorescence Stokes shift, the nature of the perturbation is very similar.

In the present paper, we describe off-resonant transient birefringence spectroscopy using the Liouville equation and discuss the molecular aspects of the observed liquid response in the time domain.[16] Transient birefringence spectroscopy is basically a pump–probe technique utilizing polarized fields.[17–22] By adding an arbitrarily controlled local oscillator field into the detector along with the nonlinearly generated signal (heterodyne detection), we can measure the modulation of the local oscillator field by the macroscopic polarization of the optical medium.[2,20,22] In particular, adjusting the phase shift of the local oscillator field to be $\pi/2$ with respect to the probe field makes it possible to measure the change of the refractive index with respect to time. Since polarized fields in the laboratory frame are used, the rotational anisotropic contribution to the signal must be included. Cho *et al.*[23] have recently presented the tensorial response function representing the rotational contribution to four-wave mixing spectroscopy. For resonant excitation, a theoretical description of the dichroism and birefringence spectroscopies is given in Ref. 23.

Off-resonant transient birefringence (or the optical Kerr effect) of pure liquids and solutions induced by subpicosecond pulses has been studied by several groups. Ultrafast responses in liquids were observed with time scales as short as tens of femtoseconds. For example, Kenney-Wallace and co-workers[2] measured femtosecond optical

[a]Present address: Department of Chemistry, University of Pennsylvania, Philadelphia, Pennsylvania.

 0021-9606/93/99(4)/2410/19/$6.00 

Kerr effect responses in several simple liquids such as $CS_2$ and acetonitrile. Nelson and co-workers[6,7] carried out time-resolved femtosecond stimulated Raman scattering experiments to study coherent vibrational dynamics in solution. In coherent Raman spectroscopies [namely, impulsive stimulated Raman scattering (ISRS) or off-resonant transient grating spectroscopy[24,25]], two pump pulses create a spatial grating in the sample. A delayed probe pulse is then diffracted by this spatial grating. The coherent Raman signal is thus proportional to the square of the induced nonlinear polarization.[7,16] In contrast to coherent Raman techniques, the heterodyne-detected optical Kerr signal depends linearly on the induced nonlinear polarization.[2–5,16,23] This provides enhanced sensitivity compared to coherent Raman techniques. A comparison between the two experimental techniques will be given in Sec. VIII.

The signals observed in the various time-domain spectroscopies mentioned above can be described in terms of the corresponding response functions. In general the total response function consists of both electronic and nuclear contributions.[26] Within the Born–Oppenheimer approximation the electronic response may be considered instantaneous.[26] However, during the pump pulse it generally makes the dominant contribution to the signal and must be removed from the convoluted total signal for accurate analysis of the nuclear response (see Sec. V). In the heterodyne detected optical Kerr technique we are not aware of any simple experimental method which allows direct measurement of the pure nuclear contribution. However, as the symmetries of the third-order electronic and nuclear response tensors differ[26] it is possible by adjusting the polarizations of the pump and probe pulses to select the nuclear or electronic response in coherent Raman scattering or transient-grating spectroscopy.[27,28]

The molecular phenomena underlying the nuclear part of the response have been discussed by many authors.[2,4–6,29,30] The long time portion of the signal is generally regarded as arising from diffusive reorientational motion. The shorter time behavior contains contributions from the collective polarizability of the system. This latter quantity contains contributions from individual molecules and from interaction-induced effects.[30–33] One possible description of these collective motions of liquids is as a collection of intermolecular vibrational modes, for example, liquid normal modes.[2,5,29,34] Such a description will only have validity on short time scales, however, the ultrafast responses observed in a variety of spectroscopic experiments (for example, fluorescence Stokes shift,[13,14] photon echo,[35–40] optical Kerr,[1–5,14,29] impulsive stimulated Raman scattering,[6,7,24,25] three pulse scattering[36(c),41]) suggest that a short time description may be adequate to understand these dynamical phenomena.

In the present paper, we develop a theoretical description for off-resonant birefringence spectroscopy. A master equation for the propagated doorway state is derived starting with the Liouville equation (Sec. II). The birefringence signal is described by the response function of the tensorial molecular polarizability in Sec. III. In Sec. IV, we expand the polarizability up to first order in the relevant coordinate and subsequently apply the Brownian oscillator model for the coordinate response function. In order to describe the collective nature of the dynamics of total polarizability of the sample, we introduce a set of intermolecular vibrational coordinates. We further assume that the long-time decaying component of the signal can be described by a diffusive molecular reorientational motion and that the dynamics of the intermolecular vibrational coordinates defined around a liquid configuration is described by underdamped oscillatory motions averaged over liquid configurations. Relationships between off-resonant transient birefringence and spontaneous and coherent Raman spectroscopies are discussed in Sec. V. The relationships derived are general and independent of any dynamical models. Here the spontaneous Raman scattering includes both the depolarized light scattering and vibrational Raman scattering. Experimental methods for measuring transient birefringence are summarized in Sec. VI. We describe the numerical technique of deconvolution in Sec. VII. Experimental transient birefringence data and simulations of both the spontaneous and coherent Raman signals are given in Sec. VIII. Finally, discussion and summary follow in Secs. IX and X.

## II. MASTER EQUATION FOR THE DOORWAY WAVE PACKETS IN TRANSIENT BIREFRINGENCE

For a two electronic-level system with a ground state $g$ and an excited state $e$ located at position $\mathbf{r}$, the molecular density matrix is in general written as

$$\rho(\mathbf{r},t)=\sum_{\alpha,\beta=g,e}|\alpha\rangle\rho_{\alpha\beta}(\mathbf{r},t)\langle\beta| \tag{2.1}$$

where $\rho_{\alpha\beta}(\mathbf{r},t)$ is an operator in the molecular nuclear space. The diagonal matrix elements represent nuclear dynamics in the electronic ground and excited states, whereas the off-diagonal elements correspond to electronic coherence.

Consider the following external field:

$$\mathbf{E}_T(\mathbf{r},t)=\mathbf{E}_1(\mathbf{r},t)+\mathbf{E}_2(\mathbf{r},t)+\mathbf{E}_{\mathrm{LO}}(\mathbf{r},t) \tag{2.2a}$$

with

$$\begin{aligned}\mathbf{E}_1(\mathbf{r},t)&=\mathbf{E}_1(t)\exp(i\mathbf{k}_1\mathbf{r}-i\omega_1 t)+\text{c.c.},\\ \mathbf{E}_2(\mathbf{r},t)&=\mathbf{E}_2(t-t_d)\exp(i\mathbf{k}_2\mathbf{r}-i\omega_2 t)+\text{c.c.},\\ \mathbf{E}_{\mathrm{LO}}(\mathbf{r},t)&=\mathbf{E}_{\mathrm{LO}}(t-t_d)\exp(i\mathbf{k}_{\mathrm{LO}}\mathbf{r}-i\omega_{\mathrm{LO}}t+i\psi)+\text{c.c.}\end{aligned} \tag{2.2b}$$

Here $E_1(\mathbf{r},t)$, $E_2(\mathbf{r},t)$, and $E_{\mathrm{LO}}(\mathbf{r},t)$ denote the pump, probe, and local oscillator fields, respectively. c.c. denotes the complex conjugate. The local oscillator field is optically phase shifted by $\psi$ with respect to the probe field.

We assume that the pump and the probe fields are separated in time so that the optical process is sequential. The pump field creates a doorway wave packet of the density matrix which then interacts with the probe. In this section we consider the description of the doorway preparation and evolution. In the next section we discuss the interaction with the probe and the signal.

We first consider the preparation of the doorway state, which is created by the interaction of the optical medium with the pump field. The Liouville equation for the density matrix is

$$\frac{d}{dt}\rho(\mathbf{r},t)=-\frac{i}{\hbar}[H-\mathbf{E}_1(\mathbf{r},t)\cdot\mathbf{V},\rho(\mathbf{r},t)], \tag{2.3}$$

where the Hamiltonian $H$ and electronic transition dipole $\mathbf{V}$ in the electric dipole approximation are

$$H=|g\rangle H_g\langle g|+|e\rangle(H_e+\omega_{eg})\langle e|,$$

$$\mathbf{V}=\boldsymbol{\mu}(\mathbf{q})(|g\rangle\langle e|+|e\rangle\langle g|), \tag{2.4}$$

where $\boldsymbol{\mu}(\mathbf{q})$ is the coordinate-dependent dipole operator.

We further define Liouville space operators as follows:

$$L_{\alpha\beta}A\equiv[H_\alpha A-AH_\beta]/\hbar,$$

$$\bar{\mathbf{V}}_{\alpha\beta,\alpha'\beta'}A\equiv[\delta_{\beta\beta'}(1-\delta_{\alpha\alpha'})\boldsymbol{\mu}A-A\boldsymbol{\mu}(1-\delta_{\beta\beta'})\delta_{\alpha\alpha'}]/\hbar,$$

$$G_{\alpha\beta}(t)A\equiv\exp(-iH_\alpha t/\hbar)A\exp(iH_\beta t/\hbar). \tag{2.5}$$

Here $G_{\alpha\beta}(t)$ represents the Green function associated with the Liouville operator $L_{\alpha\beta}$. Inserting the formal solution of the Liouville equation for the off-diagonal density matrix elements into the Liouville equation for $\rho_{gg}(\mathbf{r},t)$, we obtain the generalized master equation for the diagonal density matrix elements[16]

$$\frac{d}{dt}\rho_{gg}(\mathbf{r},t)=-iL_{gg}\rho_{gg}(\mathbf{r},t)-\int_{-\infty}^{t}d\tau\,K_{gg,gg}(t,\tau)\rho_{gg}(\mathbf{r},\tau)-\int_{-\infty}^{t}d\tau\,K_{gg,ee}(t,\tau)\rho_{ee}(\mathbf{r},\tau) \tag{2.6}$$

with the time-dependent relaxation kernels;

$$K_{gg,gg}(t,\tau)=\exp\{-i\omega_{eg}(t-\tau)\}\mathbf{E}_1(\mathbf{r},t)\mathbf{E}_1(\mathbf{r},\tau):\bar{\mathbf{V}}_{gg,eg}\otimes G_{eg}(t-\tau):\bar{\mathbf{V}}_{eg,gg}+\exp\{i\omega_{eg}(t-\tau)\}\times\mathbf{E}_1(\mathbf{r},t)\mathbf{E}_1(\mathbf{r},\tau):\bar{\mathbf{V}}_{gg,ge}\otimes G_{ge}(t-\tau)\bar{\mathbf{V}}_{ge,gg}, \tag{2.7a}$$

$$K_{gg,ee}(t,\tau)=\exp\{-i\omega_{eg}(t-\tau)\}\mathbf{E}_1(\mathbf{r},t)\mathbf{E}_1(\mathbf{r},\tau):\bar{\mathbf{V}}_{gg,eg}\otimes G_{eg}(t-\tau)\bar{\mathbf{V}}_{eg,ee}+\exp\{i\omega_{eg}(t-\tau)\}\times\mathbf{E}_1(\mathbf{r},t)\mathbf{E}_1(\mathbf{r},\tau):\bar{\mathbf{V}}_{gg,ge}\otimes G_{ge}(t-\tau)\bar{\mathbf{V}}_{ge,ee}. \tag{2.7b}$$

Here the double vertical dots denote the usual contraction operator. $\otimes$ is the direct (tensor) product. The adiabatic motion of the system in the ground electronic state is described by the first term on the right-hand side of Eq. (2.6). $K_{gg,gg}(t,\tau)$ represents the nuclear relaxation processes after the interaction with the external pump field and also the loss of the ground state population to the excited electronic state. On the other hand, $K_{gg,ee}(t,\tau)$ represents population transfer from the excited electronic state to the ground electronic state.

We consider a situation when there is a separation of time scale between populations and electronic coherences. This is usually the case in the presence of fast dephasing or when the light is off-resonant. In this case the field envelope $E(\tau)$ and the populations $\rho_{gg}(\tau)$, $\rho_{ee}(\tau)$ vary little during the coherence time. In the second and the third terms on the right-hand side of Eq. (2.6), the integrand includes fast varying quantities such as $\exp[i(\omega_1\pm\omega_{eg})(t-\tau)]$. Thus we may approximate the electric field and the diagonal density matrix element by

$$\mathbf{E}_1^*(t)\mathbf{E}_1(\tau)\cong|E_1(t)|^2\hat{e}_1\hat{e}_1 \tag{2.8a}$$

and

$$\rho_{\alpha\alpha}(\mathbf{r},\tau)\cong\rho_{\alpha\alpha}(\mathbf{r},t)\quad\text{for }\alpha=g,e, \tag{2.8b}$$

where $\hat{e}_1$ represents the unit vector defining the polarization direction of the pump field. Neglecting the nuclear dynamics during the electronic coherence $G_{\alpha\beta}(t-\tau)$, we obtain

$$\int_{-\infty}^{t}d\tau\exp\{i(\omega_1\pm\omega_{eg})(t-\tau)\}G_{eg}(t-\tau)=\frac{i}{\omega_1\pm\omega_{eg}+i\gamma}, \tag{2.9}$$

where $\gamma$ is the electronic dephasing time.

Using Eqs. (2.7)–(2.9), the generalized master equation [Eq. (2.6)] simplifies to

$$\frac{d}{dt}\rho_{gg}(\mathbf{r},t)=-iL_{gg}\rho_{gg}(\mathbf{r},t)+i|E_1(t)|^2\hat{e}_1\hat{e}_1:\{\tilde{\alpha}(\omega_1)\rho_{gg}(\mathbf{r},t)-\rho_{gg}(\mathbf{r},t)\tilde{\alpha}^*(\omega_1)\}+2|E_1(t)|^2[\mathrm{Im}(A(\omega_1))]\times\hat{e}_1\hat{e}_1:\frac{\boldsymbol{\mu}\otimes\rho_{ee}(\mathbf{r},t)\boldsymbol{\mu}}{\hbar} \tag{2.10}$$

with

$$A(\omega)\equiv\frac{1}{\omega_{eg}+\omega-i\gamma}+\frac{1}{\omega_{eg}-\omega-i\gamma}, \tag{2.11a}$$

$$\tilde{\alpha}(\omega)\equiv\frac{A(\omega)}{\hbar}\boldsymbol{\mu}\otimes\boldsymbol{\mu}, \tag{2.11b}$$

where $\mathrm{Im}[A(\omega)]$ denotes the imaginary part of $A(\omega)$. $\tilde{\alpha}(\omega)$ *is the frequency-dependent second-rank polarizability tensor.* As can be seen in Eqs. (2.11), the polarizability tensor is a complex.

We reiterate that the master equation (2.10) is valid either when the electronic dephasing processes are very fast or when the excitation is off-resonant. In either case the relevant time scale in the integration in Eq. (2.9) is very short, which justifies the neglect of nuclear dynamics.

## III. MOLECULAR RESPONSE FUNCTION FOR OFF-RESONANT TRANSIENT BIREFRINGENCE

For off-resonance excitation, the dephasing rate $\gamma$ is negligible compared with $|\omega_{eg}\pm\omega_1|$. Furthermore, the

dephasing term is in general frequency dependent and rapidly vanishes as the detuning is increased. Then $A(\omega)$ defined by Eq. (2.11a) becomes pure real

$$A(\omega)\cong\frac{1}{\omega_{eg}+\omega}+\frac{1}{\omega_{eg}-\omega}. \tag{3.1}$$

Since $\mathrm{Im}(A)$ vanishes, the excited state density matrix element in Eq. (2.10) is effectively decoupled from the ground state density matrix element. Consequently, no population in the excited state is created by an off-resonant field. This is of course to be expected on physical grounds.

The equation of motion for the ground state density matrix can then be recast using an effective Hamiltonian

$$\frac{d}{dt}\rho_{gg}(\mathbf{r},t)=-\frac{i}{\hbar}[H_{\mathrm{eff}}(t),\rho_{gg}(\mathbf{r},t)], \tag{3.2}$$

with the effective Hamiltonian

$$H_{\mathrm{eff}}(t)=H_g+V_{\mathrm{int}}(t), \tag{3.3}$$

$$V_{\mathrm{int}}(t)=-|E_1(t)|^2\hat{e}_1\hat{e}_1:\tilde{\alpha}(\omega_1). \tag{3.4}$$

For sufficiently weak pump fields, to second order with respect to the pump field [or to the first order with respect to $V_{\mathrm{int}}(t)$] we get

$$\rho_{gg}^{(2)}(t)=\left(\frac{-1}{i\hbar}\right)\int_0^\infty dt_1|E_1(t-t_1)|^2\hat{e}_1\hat{e}_1:G_{gg}(t_1)\times[\tilde{\alpha}(\omega_1),\rho_{\mathrm{eq}}]. \tag{3.5}$$

where $\rho_{\mathrm{eq}}$ denotes the equilibrium density matrix. Note that $\rho_{gg}^{(2)}(t)$ does not depend on $\mathbf{r}$ since the spatial dependence of the fields cancels in $|E_1(t-t_1)|^2$. As can be seen in Eq. (3.5), the second order ground state density matrix element is obtained by the convolution of the propagated polarizability in the ground electronic potential surface with the pump field intensity.

In order to obtain the transient birefringence signal, we evaluate the $\mathbf{k}_2$ component of the polarization, which is defined as

$$\mathbf{P}^{(3)}(\mathbf{k}_2,t)=\int d\mathbf{r}\exp(-i\mathbf{k}_2\mathbf{r}+i\omega_2 t)\mathbf{P}^{(3)}(\mathbf{r},t). \tag{3.6}$$

Here we assumed that $\mathbf{k}_{\mathrm{LO}}=\mathbf{k}_2$ and $\omega_{\mathrm{LO}}=\omega_2$. The position- and time-dependent polarization is given by the expectation value of the dipole operator:

$$\mathbf{P}^{(3)}(\mathbf{r},t)=\mathrm{Tr}[\mu\{\rho_{eg}^{(3)}(\mathbf{r},t)+\rho_{ge}^{(3)}(\mathbf{r},t)\}], \tag{3.7}$$

where the off-diagonal density matrix elements are similarly given by Eq. (2.6) with replacing the pump field by the probe field and neglecting the excited state population

$$\rho_{eg}^{(3)}(\mathbf{r},t)=i\int_{-\infty}^{t}d\tau\exp\{-i\omega_{eg}(t-\tau)\}\mathbf{E}_2(\mathbf{r},\tau)\times G_{eg}(t-\tau)\bar{\mathbf{V}}_{eg,gg}\rho_{gg}^{(2)}(\mathbf{r},\tau). \tag{3.8}$$

Since the time scales of the probe (or local oscillator) field and nuclear dynamics are negligibly short compared with $\omega_{eg}\pm\omega_{2\text{ or LO}}$, we invoke approximations given in Eqs. (2.8) and (2.9). We then have

$$\mu\{\rho_{eg}^{(3)}(\mathbf{r},t)+\rho_{ge}^{(3)}(\mathbf{r},t)\}=\exp(i\mathbf{k}_2\mathbf{r}-i\omega_2 t)\mathbf{E}_2(t-t_d)\cdot\left[\frac{\rho_{gg}^{(2)}(\mathbf{r},t)\mu\otimes\mu}{\hbar(\omega_{eg}+\omega_2)}+\frac{\mu\otimes\mu\rho_{gg}^{(2)}(\mathbf{r},t)}{\hbar(\omega_{eg}-\omega_2)}\right]. \tag{3.9}$$

Therefore, the $\mathbf{k}_2$ component of the polarization can be written in the form

$$\mathbf{P}(\mathbf{k}_2,t)=\mathbf{E}_2(t-t_d)\cdot\mathrm{Tr}[\tilde{\alpha}(\omega_2)\rho(t)]. \tag{3.10}$$

*The polarization is determined by the expectation value of the molecular electronic polarizability with respect to the propagated doorway state.*

The heterodyne-detected birefringence signal, which is measured by controlling the phase shift $\psi$ of the local oscillator field to be $\pi/2$, is given as[22]

$$S(t_d)=2\,\mathrm{Re}\int_{-\infty}^{\infty}dt\,\mathbf{E}_{\mathrm{LO}}^*(t-t_d)\cdot\mathbf{P}(\mathbf{k}_2,t). \tag{3.11}$$

By substituting Eq. (3.10) into Eq. (3.11), the off-resonant birefringence tensorial signal is

$$\tilde{\tilde{S}}(t_d)=2\int_{-\infty}^{\infty}dt\,E_{\mathrm{LO}}^*(t-t_d)E_2(t-t_d)\times\int_0^\infty dt_1|E_1(t-t_1)|^2\tilde{\tilde{\chi}}(t_1) \tag{3.12}$$

with

$$\tilde{\tilde{\chi}}(t)\equiv\left\langle\frac{i}{\hbar}[\tilde{\alpha}(\omega_2,t),\tilde{\alpha}(\omega_1,0)]^{\ddagger}\right\rangle. \tag{3.13}$$

Here the commutator $[\cdots]^{\ddagger}$ in the above equation is defined as

$$[\tilde{\alpha}(\omega_2,t_1),\tilde{\alpha}(\omega_1,0)]^{\ddagger}=\tilde{\alpha}(\omega_2,t_1)\otimes\tilde{\alpha}(\omega_1,0)-\tilde{\alpha}(\omega_1,0)\otimes\tilde{\alpha}(\omega_2,t_1), \tag{3.14}$$

where

$$\tilde{\alpha}(\omega,t)=G_{gg}(t)\tilde{\alpha}(\omega).$$

The homodyne-detected transient birefringence signal is given by

$$S_{\mathrm{homo}}(t_d)=\int_{-\infty}^{\infty}dt\,\mathbf{P}^*(\mathbf{k}_2,t)\cdot\mathbf{P}(\mathbf{k}_2,t). \tag{3.15}$$

Inserting Eq. (3.10) into (3.15), the homodyne-detected tensorial signal is written as

$$\tilde{\tilde{S}}_{\mathrm{homo}}(t_d)=\int_{-\infty}^{\infty}dt|E_2(t-t_d)|^2\times\left\{\int_0^\infty dt_1|E_1(t-t_1)|^2\tilde{\tilde{\chi}}(t_1)\right\}^2. \tag{3.16}$$

Equations (3.12) and (3.13) are the main results in this section. The off-resonant birefringence signal is given by the response function of the frequency-dependent polarizability tensor. Thus the fourth-rank tensorial signal de-

scribes all possible polarization directions. *Equation (3.13) allows us to relate the birefringence signal to intramolecular and intermolecular nuclear motions which enter through their effects on the polarizability.*

## IV. APPLICATION OF BROWNIAN OSCILLATOR AND ROTATIONAL DIFFUSION MODELS TO THE NUCLEAR RESPONSE FUNCTION

First, we consider molecules with a general polarizability tensor, and briefly sketch the calculation of the response function by expanding the polarizability in terms of intra- and intermolecular vibrational coordinates in Sec. IV A. In Sec. IV B, we shall consider a symmetric top molecule, and calculate a single molecular contribution to the response function for various polarization configurations, which are relevant for off-resonant birefringence and coherent Raman scattering. In Sec. IV C, we introduce the Brownian oscillator model for the intra- and intermolecular vibrational modes. It should be noted that throughout this section we present a dynamical model to describe both the short-time vibrational and the long-time diffusive behaviors of the liquid response.

By including the dipole–induced-dipole interactions, the collective polarizability of the interacting sample is in general expressed as[32,33]

$$\tilde{\alpha}(t)=\sum_i [\tilde{\alpha}_i(t)+\Delta\tilde{\alpha}_i(t)], \tag{4.1}$$

where the interaction induced polarizability $\Delta\tilde{\alpha}_i(t)$ is

$$\Delta\tilde{\alpha}_i(t)=\tilde{\alpha}_i\cdot\sum_{j\neq i} T_{ij}\cdot\tilde{\alpha}_j\cdot\bar{T}_{ji}\cdot\tilde{\alpha}_i+\tilde{\alpha}_i\cdot\sum_{j\neq i}\bar{T}_{ij}\cdot\tilde{\alpha}_j \tag{4.2}$$

with

$$\bar{T}_{ij}=T_{ij}+\sum_m T_{im}\cdot\tilde{\alpha}_m\cdot T_{mj}+\cdots \quad (i\neq j). \tag{4.3}$$

Here $\tilde{\alpha}_i$ denotes an isolated molecular polarizability, and $T_{ij}(\mathbf{r}_{ij})$ is the dipole–dipole interaction tensor

$$T_{ij}(\mathbf{r}_{ij})=\frac{3\hat{r}_{ij}\hat{r}_{ij}-\hat{I}}{r_{ij}^3} \tag{4.4}$$

$\hat{r}_{ij}$ is a unit vector in the direction $\mathbf{r}_i-\mathbf{r}_j$, where $\mathbf{r}_i$ and $\mathbf{r}_j$ are the positions of the centers of mass of the $i$th and $j$th molecules. The first term in the expression for the induced polarizability [Eq. (4.2)] is the reaction-field (self-) induced polarizability. The second term in Eq. (4.2) is the polarizability induced by the fields from all the other molecules in the sample. The gas-phase polarizability tensor terms in the collective polarizability depends only on the molecular orientation of the $i$th molecule when the molecular polarizability is anisotropic. On the other hand, all the induced polarizabilities [the second term in Eq. (4.1)] are determined by both the translational and rotational nuclear degrees of freedom, since the dipole–induced-dipole interaction tensor is a function of $\mathbf{r}_{ij}(t)$.

### A. Expansion of the polarizability in nuclear coordinates

Our focus in this paper is on the short-time dynamics for which a natural description is in terms of intermolecular vibrational modes. However, the experimental signals contain, in general, a long-time contribution arising from diffusive orientational motion which must therefore be included in the theoretical description. Using the weak dependence of the polarizability on nuclear coordinates, we expand the collective polarizability with respect to the equilibrium configuration $\mathbf{y}^0$

$$\tilde{\alpha}(\mathbf{y})=\tilde{\alpha}^0(\mathbf{y}^0)+\sum_j\left(\frac{\partial\tilde{\alpha}}{\partial y_j}\right)_{\mathbf{y}^0} y_j+\cdots. \tag{4.5}$$

Here the nuclear coordinates $y_j$ stand for $\mathbf{q}$, $\mathbf{Q}$, and $\nu$ representing intramolecular vibrational coordinates, intermolecular vibrational coordinates, and the molecular rotational coordinates respectively. Since we are interested in short time dynamics, we shall expand the polarizability to first order with respect to the nuclear coordinates

$$\tilde{\alpha}(\mathbf{q},\nu,\mathbf{Q})=\tilde{\alpha}^0(\mathbf{q}^0,\nu^0,\mathbf{Q}^0)+\tilde{\alpha}^I(t)+\tilde{\alpha}^{II}(t) \tag{4.6}$$

with

$$\tilde{\alpha}^I(t)=\tilde{\alpha}_0^I[\nu(t)]+\sum_i\left\{\frac{\partial\tilde{\alpha}[\nu(t)]}{\partial q_i}\right\}_{\mathbf{y}^0} q_i(t), \tag{4.7a}$$

$$\tilde{\alpha}^{II}(t)=\sum_j\left(\frac{\partial\tilde{\alpha}}{\partial Q_j}\right)_{\mathbf{y}^0} Q_j(t). \tag{4.7b}$$

Here $\tilde{\alpha}^I$ and $\tilde{\alpha}^{II}$ are *intramolecular* and *intermolecular* contributions, respectively. $\tilde{\alpha}_0^I[\nu(t)]$ represents an orientation-dependent molecular polarizability of a rigid molecule. The intramolecular vibrational contributions are represented by the second term in Eq. (4.7a). The first term on the right-hand side of Eq. (4.6) is a constant independent of nuclear coordinates and therefore does not contribute to the response function $\tilde{\tilde{\chi}}(t)$.

By treating rotational motions classically, the response function for the off-resonant birefringence signal then becomes

$$\tilde{\tilde{\chi}}(t)\equiv\tilde{\tilde{Y}}_0^R(t)+\sum_i\left\langle\frac{i}{\hbar}[q_i(t),q_i(0)]\right\rangle\tilde{\tilde{Y}}_i(t)+\sum_j\left[\left(\frac{\partial\tilde{\alpha}}{\partial Q_j}\right)_{\mathbf{y}^0}\otimes\left(\frac{\partial\tilde{\alpha}}{\partial Q_j}\right)_{\mathbf{y}^0}\right]\times\left\langle\frac{i}{\hbar}[Q_j(t),Q_j(0)]\right\rangle \tag{4.8}$$

with

$$y_j(t)=\exp(iH_g t/\hbar)y_j \exp(-iH_g t/\hbar)$$

$$(y_j(t)=q_j(t),Q_j(t)),$$

where $\tilde{\tilde{Y}}_i(t)$ is the fourth-rank tensorial function describing the rotational propagation of the molecular orientation in the laboratory frame.[23] The approximation made in writing Eqs. (4.5) and (4.8) is equivalent to partitioning the intermolecular modes into two groups—a small subset that will eventually lead to the diffusive orientational motion and the remainder whose short time behavior we are interested in. This division, which certainly an approximation, seems reasonable in light of the simulation results of Ohmine and Tanaka.[42] They found that the lowest frequency intermolecular vibrational modes are the ones that almost always lead to structural transitions. In a recent instantaneous normal mode calculation of liquid water[43] we have found that modes with low frequencies ($<50$ $cm^{-1}$) have significantly larger amplitude motions than higher frequency modes and are therefore more likely to be found displaced from their local equilibrium position. Thus the aim of the separation of intermolecular coordinates and rotational coordinates is to have one set (the major group) whose short time behavior is handled correctly and a second group whose long time behavior is described appropriately. Since the intermolecular coordinates given in Eq. (4.7b) are defined around a liquid configuration, their dynamical evolution does not contain any information on changes in the local liquid structure. Nor does it describe slowly varying diffusive motions, whose time scales are usually larger than a picosecond in liquids.

Returning to the rotational contribution $\tilde{\tilde{Y}}_i(t)$ is defined as[23]

$$\tilde{\tilde{Y}}_i(t)=\int d\nu\, d\nu_0 \left[\frac{\partial\tilde{\alpha}(\nu)}{\partial q_i}\right]_{y^0} \otimes W(\nu,t;\nu_0) \times\left[\frac{\partial\tilde{\alpha}(\nu_0)}{\partial q_i}\right]_{y^0} W_0(\nu_0), \tag{4.9}$$

where $\nu_0$ and $\nu$ represent the Euler angles defining the molecular orientation at $t=0$ and $t=t$. $W_0(\nu_0)$ is the initial distribution of $\nu_0$. For an isotropic medium, $W_0(\nu_0)=1/8\pi^2$. $W(\nu,t;\nu_0)$ is the conditional probability function of finding $\nu=\nu$ at $t=t$, being $\nu_0$ at $t=0$. The second-rank tensor $(\partial\tilde{\alpha}(\nu)/\partial q_i)_{y^0}$ is defined by the molecular orientation specified by the Euler angles $\nu$ in the laboratory coordinate system. Since the first term in Eq. (4.8) is treated classically when the response function is calculated, the purely rotational contribution to the total response function, $\tilde{\tilde{\chi}}(t)$, should be replaced by the corresponding classical response function[44–46]

$$\left\langle \frac{i}{\hbar}\{\tilde{\alpha}_0^I[\nu(t)],\tilde{\alpha}_0^I[\nu(0)]\}\right\rangle \propto -\frac{\theta(t)}{k_B T}\frac{\partial}{\partial t}\tilde{\tilde{Y}}_0(t)\equiv\tilde{\tilde{Y}}_0^R(t),$$

where

$$\tilde{\tilde{Y}}_0^R(t)\equiv -\frac{\theta(t)}{k_B T}\frac{\partial}{\partial t}\int d\nu\, d\nu_0\, \tilde{\alpha}_0^I(\nu) \otimes W(\nu,t;\nu_0)\tilde{\alpha}_0^I(\nu_0)W_0(\nu_0). \tag{4.10}$$

The first equation can be obtained by expanding Eq. (R1) for classical limit ($\hbar\omega\ll k_B T$) (see Ref. 44). Here $\theta(t)$ is a step function. This approximation would be valid for diffusive rotational motion, since the rotational time scale (i.e., rotational time constant) is usually much longer than $\hbar/k_B T$ (160 fs at room temperature). Equations (3.12) and (3.13) can be used to develop a complete quantum description of rotation. This is however usually not necessary in the condensed phase. Finally we note that expression (4.10) correctly begins at zero at $t=0$, builds up, and then turns over and smoothly turns into diffusive motion at longer times. This is because the inertial term is included in the dynamical equation of motion, e.g., the Fokker–Planck equation. The initial rising component of Eq. (4.10) is governed by the damping rate of the angular velocity, which is faster than the rotational damping process.

### B. A single-molecular contribution to the polarizability response function

If we ignore both the dipole–induced-dipole interaction contribution to a single molecular polarizability and cross response functions including two polarizabilities, the response function in Eq. (3.13) reduces to $\langle i/\hbar[\tilde{\alpha}^I(t),\tilde{\alpha}^I(0)]\rangle$, where $\tilde{\alpha}(t)$ is an effective polarizability of a molecule. The first and the second terms in Eq. (4.8) correspond to the pure rotational and intramolecular rovibrational contributions of a single molecule. *For a symmetric top molecule*, let $\mathbf{u}$ be a unit vector which lies along the symmetry axes. The molecular polarizability tensor $\tilde{\alpha}$ can be divided into its scalar part $\alpha$ and its anisotropic part $\tilde{\beta}$ so that[47]

$$\tilde{\alpha}=\alpha\tilde{I}+\tilde{\beta}, \tag{4.11}$$

where $\alpha=(\mathrm{Tr}\,\tilde{\alpha})/3$, $\mathrm{Tr}\,\tilde{\beta}=0$, and $\hat{I}$ denotes a $3\times3$ unit tensor. Here Tr denotes a trace. We can divide the response function, $\langle i/\hbar[\tilde{\alpha}^I(t),\tilde{\alpha}^I(0)]\rangle$, into its isotropic and anisotropic parts (see Appendix A)

$$\chi_{\mathrm{iso}}^I(t)=\left\langle \frac{i}{\hbar}[\alpha(t),\alpha(0)]\right\rangle, \tag{4.12a}$$

$$\chi_{\mathrm{aniso}}^I(t)=\left\langle \frac{i}{\hbar}[\beta(t),\beta(0)]\right\rangle \langle P_2[\mathbf{u}(0)\cdot\mathbf{u}(t)]\rangle, \tag{4.12b}$$

where $\alpha(t)$ and $\beta(t)$ defined in Eq. (A2) are isotropic and anisotropic polarizabilities of a molecule in the Heisenberg picture. It should be noted that since we treated the rotational motion classically the single molecular response function is a product of the response function of the anisotropic part of the polarizability and the correlation function of the molecular orientation, $\langle P_2[\mathbf{u}(0)\cdot\mathbf{u}(t)]\rangle$. For example, if the pump and probe beams are polarized along

$j$ and $l$ axes, respectively, the corresponding response function for off-resonant birefringence is given as [see Eq. (A8)]

$$\chi^I_{lljj}(t)=\chi^I_{\rm iso}(t)+\frac{4}{45}P_2(\mathbf{n}_j\cdot\mathbf{n}_l)\chi^I_{\rm aniso}(t). \tag{4.13}$$

Here $\mathbf{n}_j$ denotes the unit vector along the laboratory $j$ axis. The relevant response functions for coherent Raman spectroscopies are in the form [see Eq. (B3)]

$$\chi^I_{ljlj}(t)=(\mathbf{n}_l\cdot\mathbf{n}_j)^2\chi^I_{\rm iso}(t)+\frac{1}{15}\left[1+\frac{1}{3}(\mathbf{n}_l\cdot\mathbf{n}_j)^2\right]\chi^I_{\rm aniso}(t). \tag{4.14}$$

#### 1. Pure rotational contribution

As discussed earlier, for a rigid molecule the rotational response function is calculated by inserting the classical reorientational correlation function into Eq. (4.10)

$$Y^R_{0,lljj}(t)=-\frac{4\theta(t)\beta^2}{45k_BT}P_2(\mathbf{n}_j\cdot\mathbf{n}_l)\frac{\partial}{\partial t}\langle P_2[\mathbf{u}(0)\cdot\mathbf{u}(t)]\rangle,$$

$$Y^R_{0,ljlj}(t)=-\frac{\theta(t)\beta^2}{15k_BT}\left[1+\frac{1}{3}(\mathbf{n}_l\cdot\mathbf{n}_j)^2\right]\times\frac{\partial}{\partial t}\langle P_2[\mathbf{u}(0)\cdot\mathbf{u}(t)]\rangle. \tag{4.15}$$

Since we consider a rigid molecule, the isotropic part in Eq. (4.12a) does not contribute to the rotational response function, that is to say, the isotropic part is rotationally invariant.

#### 2. Intramolecular rovibrational contribution

If we expand $\alpha$ and $\beta$ in the intramolecular vibrational normal coordinates of a molecule and keep the linear terms only, the isotropic and anisotropic response functions in Eqs. (4.12a) and (4.12b) are written as

$$\chi^I_{\rm iso}(t)=\sum_j\left[\frac{\partial\alpha}{\partial q_j}\right]^2_0\left\langle\frac{i}{\hbar}[q_j(t),q_j(0)]\right\rangle, \tag{4.16a}$$

$$\chi^I_{\rm aniso}(t)=\langle P_2[\mathbf{u}(0)\cdot\mathbf{u}(t)]\rangle\sum_j\left[\frac{\partial\beta}{\partial q_j}\right]^2_0\left\langle\frac{i}{\hbar}[q_j(t),q_j(0)]\right\rangle, \tag{4.16b}$$

where $[\partial\alpha/\partial q_j]_0$ and $[\partial\beta/\partial q_j]_0$ are the first-order expansion coefficients at the equilibrium internuclear separation in a molecule. Inserting Eqs. (4.15) and (4.16) into (4.13) and (4.14), we can express various tensor elements of the single molecular contributions to response function.

### C. Brownian oscillator model for intra- and intermolecular vibrational contributions

In Sec. IV A, we expanded the collective polarizability in terms of both the intra- and intermolecular vibrational coordinates. Although for polyatomic molecules the interpretation of the Raman spectrum via normal mode analysis is standard, the use of a normal mode description of liquids to understand their short time dynamical behavior is comparatively recent. Based on the ultrafast nature (about 100 fs) of the material response, we consider a collection of the intermolecular vibrational coordinates. Although it is possible to apply the idea of separating a single molecular polarizability into isotropic and anisotropic components to the collective polarizability, we instead project the dynamical aspects of the collective polarizability onto a number of intermolecular vibrational modes. Thus the collective orientational effect is blended into the sum of the intermolecular vibrational dynamics.

We shall model the nuclear motions $y_j(=q_i,Q_j)$ by harmonic Brownian oscillators. Then $y_j$ satisfies the generalized Langevin equation

$$M_j\ddot{y}_j=-M_j\omega_j^2y_j-\int_{-\infty}^{t}d\tau\,\gamma_j(t-\tau)\dot{y}_j(\tau)+f_j(t), \tag{4.17}$$

where $\gamma_j(t)$ and $f_j(t)$ denote the time-dependent friction kernel and Gaussian random force. $M_j$ and $\omega_j$ are the reduced mass and frequency of the $j$th mode, respectively. The response functions in the Markovian approximation are given as[16]

$$\left\langle\frac{i}{\hbar}\{y_j(t)y_j-y_jy_j(t)\}\right\rangle=\frac{Z_j(t)}{M_j\Omega_j} \tag{4.18}$$

with

$$Z_j(t)=\exp(-\gamma_jt/2)\sin\Omega_jt, \tag{4.19}$$

where $y_j\in\{q_j,Q_j\}$ and $\Omega_j\equiv\sqrt{\omega_j^2-\gamma_j^2/4}$. The response function is given by the Green function of the Langevin equation. Since not only *intramolecular* Raman-active modes but also *intermolecular (collective)* modes contribute to the birefringence signal, the response function $\tilde{\tilde{\chi}}(t)$ assumes the form

$$\tilde{\tilde{\chi}}(t)\equiv\tilde{\tilde{Y}}^R_0(t)+\sum_i\frac{Z_i(t)}{M_i\Omega_i}\tilde{\tilde{Y}}_i(t)+\int d\omega\,\tilde{\tilde{\rho}}(\omega)Z(\omega,t), \tag{4.20}$$

where the fourth rank tensorial spectral density for the intermolecular contribution [the second term on the right-hand side of Eq. (4.20)] can be defined as

$$\tilde{\tilde{\rho}}(\omega)=\sum_j\left[\left(\frac{\partial\tilde{\alpha}}{\partial Q_j}\right)^{\vee}_{y_0}\otimes\left(\frac{\partial\tilde{\alpha}}{\partial Q_j}\right)_{y_0}\right]\frac{\delta(\omega-\omega_j)}{M_j\Omega_j(\omega)}. \tag{4.21}$$

$Z(\omega,t)$ are the mode frequency dependent response functions defined in Eq. (4.19). Since the intermolecular motion contributing to the birefringence signal is collective in nature, we can assume that the rotational tensor for the intermolecular modes does not affect to the time-dependent Green function $\tilde{\tilde{\chi}}(t)$. Equation (4.20) provides the formal basis for the expressions used by Cho *et al.*[29] in their analysis of solvation and optical Kerr dynamics in acetonitrile.

## V. RELATIONSHIPS BETWEEN OFF-RESONANT TRANSIENT BIREFRINGENCE AND COHERENT AND SPONTANEOUS RAMAN SPECTROSCOPIES

In the present section, we shall discuss how one experiment using a particular combination of off-resonant fields

can be related to other kinds of experiment. Since the nuclear response function denoted as $\tilde{\tilde{\chi}}(t)$ is independent of the dynamical model, the following relationships given below are general.

In a grating configuration we add another field $\mathbf{E}_2(t)$ whose wavevector is $\mathbf{k}_2$. We assume it has the same temporal profile as $E_1(t)$ but arbitrary polarization direction

$$\mathbf{E}_T(\mathbf{r},t)=\mathbf{E}_1(\mathbf{r},t)+\mathbf{E}_2(\mathbf{r},t)+\mathbf{E}_3(\mathbf{r},t) \tag{5.1}$$

with

$$\mathbf{E}_1(\mathbf{r},t)=\mathbf{E}_1(t)\exp(i\mathbf{k}_1\mathbf{r}-i\omega_1 t)+\text{c.c.},$$

$$\mathbf{E}_2(\mathbf{r},t)=\mathbf{E}_2(t)\exp(i\mathbf{k}_2\mathbf{r}-i\omega_2 t)+\text{c.c.},$$

$$\mathbf{E}_3(\mathbf{r},t)=\mathbf{E}_3(t-t_d)\exp(i\mathbf{k}_3\mathbf{r}-i\omega_3 t)+\text{c.c.},$$

where

$$\mathbf{E}_1(t)\equiv E_1(t)\hat{e}_1,\quad \mathbf{E}_2(t)\equiv E_1(t)\hat{e}_2,$$

$$\text{and } \mathbf{E}_3(t)\equiv E_3(t)\hat{e}_3. \tag{5.2}$$

Equation (3.4) is now given by[16]

$$V_{\text{int}}(\mathbf{r},t)=-2|E_1(t)|^2\{1+\cos(\mathbf{k}_1-\mathbf{k}_2)\mathbf{r}\}\hat{e}_1\hat{e}_2:\tilde{\alpha}(\omega_1). \tag{5.3}$$

In Eqs. (3.6) and (3.11), we replace $\mathbf{k}_2$ by $\mathbf{k}_s=\mathbf{k}_1-\mathbf{k}_2+\mathbf{k}_3$. We then have the following cases

(i) $\mathbf{k}_1=\mathbf{k}_2$: pump–probe, birefringence;

(ii) $\mathbf{k}_1\neq\mathbf{k}_2$ and $\mathbf{k}_1=\mathbf{k}_3$: coherent Raman.

One distinction between heterodyne-detected birefringence technique and off-resonant coherent Raman spectroscopy should be noted. In the coherent Raman spectroscopy the light scattered by the optically generated grating is measured, and the signal is thus proportional to $\mathbf{P}^*(\mathbf{k}_S,t)\cdot\mathbf{P}(\mathbf{k}_S,t)$. This is also the case of the homodyne-detected birefringence signal. On the other hand, the heterodyne-detected birefringence signal is linear in the signal field [see Eq. (3.11)]. Furthermore, making the amplitude of the local oscillator field large enhances sensitivity considerably (see Sec. VI).

### A. Comparison of conventional off-resonant birefringence with coherent Raman scattering

We shall consider a specific pulse configuration that has been widely used for off-resonant birefringence measurement, wherein the pump field is polarized along the $Z$ axis in the laboratory frame ($\hat{e}_1=\hat{Z}$) and the relative pump and probe (also local oscillator) beam polarization is adjusted to be 45° (i.e., $\hat{e}_2=\hat{e}_{\text{LO}}=(\hat{Y}+\hat{Z})/\sqrt{2}$). The heterodyne-detected birefringence signal is then determined by

$$S(t_d)=[\tilde{\tilde{S}}(t_d)]_{ZZZZ}-[\tilde{\tilde{S}}(t_d)]_{YYZZ}, \tag{5.4}$$

where we assume that the pulses are propagating along the $X$ axis in the laboratory coordinate system. Using Eqs. (3.12) and (3.16), the heterodyne- and homodyne-detected off-resonant birefringence signals in this case are given by

$$S_{\text{hetero}}(t_d)=\int_{-\infty}^{\infty}dt\,E_{\text{LO}}^*(t-t_d)E_2(t-t_d)\int_0^{\infty}dt_1\times|E_1(t-t_1)|^2\{\chi_{ZZZZ}(t_1)-\chi_{YYZZ}(t_1)\}, \tag{5.5a}$$

$$S_{\text{homo}}(t_d)=\int_{-\infty}^{\infty}dt|E_2(t-t_d)|^2\left\{\int_0^{\infty}dt_1\left|E_1(t-t_1)\right|^2\times\{\chi_{ZZZZ}(t_1)-\chi_{YYZZ}(t_1)\}\right\}^2, \tag{5.5b}$$

where

$$\chi_{ZZZZ}(t)-\chi_{YYZZ}(t)=\left\langle\frac{i}{\hbar}[\alpha_{ZZ}(\omega_2 t),\alpha_{ZZ}(\omega_1,0)]\right\rangle-\left\langle\frac{i}{\hbar}[\alpha_{YY}(\omega_2 t),\alpha_{ZZ}(\omega_1,0)]\right\rangle.$$

As can be seen above, the birefringence signal measures anisotropy created by the $Z$-polarized pump field. In particular, *for initially isotropic media the signal in this polarization configuration is related to the depolarized component of the light scattering in frequency-domain via the fluctuation-dissipation theorem (see below).*

In particular, the depolarized ($VH$), forward ($\mathbf{k}_1=\mathbf{k}_2$) component of the coherent Raman scattering measurements,[6(c)] where $\hat{e}_1\perp\hat{e}_2$, $\hat{e}_3=\hat{e}_1$, and $\hat{e}_{\text{detector}}=\hat{e}_2$, is equal to the homodyne signal given above. For simplicity, considering an impulsive limit of the probe and local oscillator fields give the following simplified relationships [see Eq. (B5)]:

$$S_{\text{hetero}}(t_d)\propto\int_0^{\infty}dt_1|E_1(t_d-t_1)|^2\{\chi_{ZZZZ}(t_1)-\chi_{YYZZ}(t_1)\}, \tag{5.6a}$$

$$S_{\text{homo}}(t_d)\propto|S_{\text{hetero}}(t_d)|^2, \tag{5.6b}$$

$$S_{\text{CR}}^{\text{depol}}(\mathbf{k}_1=\mathbf{k}_2,t_d)\propto S_{\text{homo}}(t_d), \tag{5.6c}$$

where $S_{\text{CR}}^{\text{depol}}(\mathbf{k}_1=\mathbf{k}_2,t_d)$ represents the depolarized forward coherent Raman scattering signal.

### B. Spontaneous Raman light scattering

The conventional Raman spectroscopy (depolarized Rayleigh scattering) is a frequency domain technique in which the vibrational frequencies and dephasings are measured as peaks and widths with respect to frequencies. In general, the possible number of pairs of polarization directions in light scattering experiments is 3, such as the $I_{VV}$, $I_{VH}$, and $I_{HH}$ components. Usually, $I_{VV}$ and $I_{VH}$ are called the *polarized* and *depolarized* components. $I_{HH}$ is often a linear combination of the polarized and depolarized components. The conventional Raman signal, which is the depolarized component, is the Fourier transform of the autocorrelation function of $\alpha_{YZ}$[45]

$$S_R(\omega=\omega_1-\omega_2)$$

$$= \int_{-\infty}^{\infty} dt \exp(i\omega t)\langle \alpha_{YZ}(\omega_2)\exp(-iH_g t/\hbar)$$

$$\times \alpha_{YZ}(\omega_1)\rho_{eq}\exp(iH_g t/\hbar)\rangle, \quad (5.7)$$

where $\omega_1$ and $\omega_2$ are the excitation and emission frequencies, respectively. This is then determined by the correlation function of the anisotropy of the polarizability of a group of interacting molecules.[45] By the fluctuation-dissipation theorem,[48] the imaginary part of the Fourier transform of the corresponding response function is equal to the conventional Raman spectrum as

$$S_R(\omega)[1-\exp(-\hbar\omega/k_B T)] = 2\hbar^2 \operatorname{Im}[\hat{\chi}_{YZYZ}(\omega)], \quad (5.8)$$

where

$$\operatorname{Im}[\hat{\chi}_{YZYZ}(\omega)] = \int_0^{\infty} dt\, \chi_{YZYZ}(t)\sin \omega t.$$

The time-resolved off-resonant birefringence signal can be related to the spontaneous Raman signal via Eq. (5.6).

The observed discrete quantum beats in the off-resonant transient birefringence signal result from *intramolecular* vibrational coherences in the ground electronic state. In frequency-domain spectra, these are observed as peaks at the corresponding frequencies broadened by the vibrational dephasing and rotational diffusion processes. Furthermore, the ultrafast decay within the first $\sim$100 fs should be related to the *collective* vibrational Raman mode contributions. The distribution of the low frequency modes can also be observed in the Rayleigh-wing spectra of pure liquids. In the Green function defined in Eq. (4.8), the third term is associated with this intermolecular contribution. Finally, the rotational motion of a molecule broadens the Rayleigh peak, which appears as a Lorentzian whose width is related to the rotational constant. Although the two techniques, time-domain birefringence and frequency-domain Raman spectroscopy, are directly related as discussed above, direct time-domain measurements of the material response may have some advantages as we hope to show in the following sections. In particular, the time resolved method may be superior in determining low-frequency Raman components because of its zero-background nature.

## VI. EXPERIMENT

The transient birefringence measurements were carried out using linearly polarized $\sim$30 fs optical pulses centered at 570 nm. The optical pulse was derived from 100 kHz repetition rate laser system, which originates with a cavity-dumped antiresonant ring dye laser that typically produces pulses of 60 fs FWHM and $\sim$3 nJ pulse energy at 610 nm. Amplification of a single dye laser pulse is achieved by using a two-stage single pass dye amplifier pumped by the frequency doubled output (3.5 $\mu$J at 532 nm) of an Nd:YAG regenerative amplifier at a repetition rate of 100 kHz.[49] The amplified output pulse has an average energy of 180–240 nJ. After compensation for group velocity dispersion using a pair of SF-10 prisms in a near retroreflecting geometry, the pulse is focused into a 2 mm flowing $H_2O$ cell to generate a continuum. A spatially and spectrally selected portion of continuum is amplified in a rhodamine 6G and rhodamine 570 mixture in ethylene glycol jet to produce a broad and nearly Gaussian spectrum centered at 570 nm. Selection and amplification of a 25 nm spectrum and appropriate prism compensation provides a pulse of $\sim$30 fs duration (3–4 nJ energy) for the transient birefringence measurements.

The apparatus for transient birefringence measurements is similar to that in Ref. 17. Briefly, the amplified beam was split into two portions: 95% was used as the pump and 5% as the probe. The pump and probe beams passed through two Glan–Taylor polarizers oriented at 45° with respect to each other. The pump beam was reflected to travel nearly collinearly with the probe and both beams were focused into a 1 mm pathlength flowing sample cell. The pump beam was blocked after the sample and the probe beam was collimated and directed to an analyzer polarizer, the transmission of which was detected by a photomultiplier tube (Amperex red-enhanced XP2020). The output of the photomultiplier is processed by a lock-in amplifier (SR530) that is referenced to the mechanical chopper frequency in the pump beam. The signal is recorded for each position of the delay line and stored in a computer. Care is taken to preserve the polarization of the beams in pump and probe and the extinction ratio for the probe beam is better than $10^{-6}$. In this homodyne configuration the signal is quadratic with respect to the response function of the sample.

In order to avoid the inherent complexity of analyzing a quadratic signal and provide the enhanced sensitivity necessary for measurements of the weak transient birefringence of alcohols, optical heterodyne detection was used in our experiments. A $\lambda/4$ wave plate was positioned between the two crossed polarizers, its "fast" axis is oriented to minimize total static birefringence in the probe beam. When performing heterodyne detection for transient birefringence, the $\lambda/4$ waveplate was rotated $<1°$ so that an in-quadrature local oscillator was transmitted to the detector. The amplitude is $\sim$30–40$\times$ that of the homodyne signal intensity. The transient birefringence was obtained by taking the difference between two scans,[19] each with the same amplitude of local oscillator field but the opposite signs. This $\pi$ shift of the local oscillator field was obtained by rotating the $\lambda/4$ wave plate equal amounts in opposite directions. The subtraction method has the advantage of removing the homodyne signal and any possible induced dichroism from the transient birefringence measurements. A typical signal was constructed by averaging over three pairs of scans.

The pure liquids were purchased from Aldrich in A.C.S. reagent grade (99.9%). The sample was flowed through a 1 mm pathlength cell to avoid thermal heating and lensing effects. All measurements were performed at room temperature.

## VII. NUMERICAL METHODS

Since the transient birefringence signal is a convolution of both the nuclear and electronic response functions with the pump intensity profile, it is necessary to deconvolute and separate electronic and nuclear responses. McMorrow and Lotshaw recently presented a numerical method of deconvolution and separation of the electronic and nuclear responses in Ref. 5. Here we describe a different method which is useful when the nuclear response is very fast and a single detection step (about 10 fs) is too large to completely resolve the ultrafast response. Since the laser autocorrelation function is measured independently, a consistent zero delay time cannot be maintained when switching between measurements of birefringence signal and laser autocorrelation function. In case of a rather slow response liquid such as acetonitrile or carbon disulfide ($CS_2$), the complications caused by a large detection time step and uncertainty in determining the absolute zero time are not severe. However, in ultrafast response liquids such as water, methanol, etc., the parameters extracted from Fourier transform analysis show a strong dependence on the zero time and detection time step. Here we present a numerical method to overcome this difficulty with a combination of the cubic-spline[50] and Fourier transform methods.

Let $\tilde{\tilde{\sigma}}$ represent the magnitude of the tensorial electronic response. Then the total tensorial response function $\tilde{\tilde{G}}(t)$ can be written as

$$\tilde{\tilde{G}}(t)=\tilde{\tilde{\sigma}}\delta(t)+\tilde{\tilde{\chi}}(t). \tag{7.1}$$

The nuclear response function $\tilde{\tilde{\chi}}(t)$ was discussed in the previous sections. The electronic response is instantaneous (delta function) compared to the nuclear response within the Born–Oppenheimer approximation. In particular, the measured transient birefringence signal can be simply rewritten as [see Eq. (5.5a)]

$$S(t)\cong\Delta\sigma I(t)+\int_{-\infty}^{\infty}d\tau\, I(t-\tau)\Delta\chi(\tau) \tag{7.2}$$

with

$$\Delta\sigma\equiv\sigma_{ZZZZ}-\sigma_{YYZZ}$$

and (7.3)

$$\Delta\chi(t)\equiv\chi_{ZZZZ}(t)-\chi_{YYZZ}(t).$$

Here $I(t)$ represents the laser autocorrelation function. From the causality condition on $\Delta\chi(t)$, the integration in Eq. (5.6a) can be carried out over $-\infty$ to $\infty$. Fourier transforming of Eq. (7.2) and simple algebra give

$$\begin{aligned}&\mathrm{Im}[\Delta\chi(\omega)]=\mathrm{Im}[S(\omega)/I(\omega)],\\&\mathrm{Re}[\Delta\chi(\omega)]=\mathrm{Re}[S(\omega)/I(\omega)]-\Delta\sigma.\end{aligned} \tag{7.4}$$

Since the raw signal and laser autocorrelation function are measured around time zero, the true zero times of the raw signal and instrument function differ from the very first data point ($t<0$) by $\Delta t_S$ and $\Delta t_I$, respectively (see Fig. 1). Because of uncertainties in $\Delta t_S$ and $\Delta t_I$, we need to obtain $\Delta t_S$ and $\Delta t_I$ from the measured signal and instrument response function. The time step of our data sets is usually 11 fs. This is too large to determine $\Delta t_S$ and $\Delta t_I$ accurately. Therefore, we use a cubic-spline technique to interpolate between each pair of data points. From the interpolated data points, we assign the time between the maximum point in the instrument function and the first data point to be $\Delta t_I$. This is a reasonable assumption because the instrument function is more symmetric in time than the raw signal. Using the fast Fourier transform technique, we can calculate the Fourier spectra $S(\omega)$ and $I(\omega)$

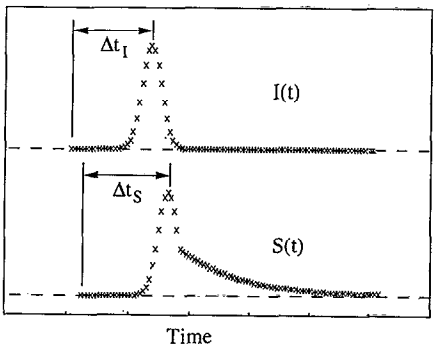


FIG. 1. Model laser autocorrelation function (top) and synthetic raw signal (bottom). The crosses represent individual data points. $\Delta t_I$ and $\Delta t_S$ denote the time gaps between the first and the maximum data points. Since the absolute zero time cannot be maintained for measurements of the laser autocorrelation function and the raw signal, $\Delta t_I$ and $\Delta t_S$ should be considered to be independent quantities. Taking $\Delta t_S$ as an adjustable parameter (we could equally well take $\Delta t_I$), the spectral density $\mathrm{Im}[\chi(\omega)]$ can be calculated (see the text for details).

$$S(\omega)=S'(\omega)\exp(i\omega\Delta t_s)$$

and (7.5)

$$I(\omega)=I'(\omega)\exp(i\omega\Delta t_I),$$

where $S'(\omega)$ and $I'(\omega)$ are the Fourier transforms of the interpolated raw signal and the laser intensity profile, respectively. Since a single time step is large, the uncertainty in choosing $\Delta t_S$ still exists. The first-order approximation is to choose the difference between the maximum point of the interpolated signal and the first data point as $\Delta t_S$. Although the electronic response contribution dominates at $t=0$, the nuclear response contribution during the rising portion ($t<0$) of the laser field induces an asymmetry in the peak at $t=0$. Therefore, we now consider $\Delta t_S$ as a parameter. A criterion for determining $\Delta t_S$ is to make the base line of $\mathrm{Im}[\chi(\omega)]$ flat and close to zero. Obtaining $S(\omega)$ and $I(\omega)$ and inserting these results into Eq. (7.4) gives the complex spectral density.

Here it should be emphasized that the spectral density obtained by this method is independent of the dynamical models discussed in the previous section. Thus the numerical procedure described above should prove useful for extracting nuclear responses from off-resonant transient birefringence measurements, and testing the validity of the theoretical model discussed above.

TABLE I. Values of the parameter $\omega_c$ obtained by fitting the experimental spectral densities to the from $\rho_{\rm bir}(\omega) \propto \omega \exp(-\omega/\omega_c)$.

| Liquid | $\omega_c$ ($cm^{-1}$) |
|---|---|
| $CH_3CN$ | 31 |
| DMSO | 36 |
| $CHCl_3$ | 20 |
| Methanol | 39 |
| Ethanol | 39 |
| Propanol | 37 |
| Butanol | 33 |
| Pentanol | 35 |
| Hexanol | 35 |
| Octanol | 33 |

## VIII. TRANSIENT BIREFRINGENCE MEASUREMENTS OF VARIOUS PURE LIQUIDS AND COMPARISONS WITH SPONTANEOUS AND COHERENT RAMAN SPECTROSCOPIES

In this section, we present transient birefringence signals for acetonitrile, dimethyl sulfoxide (DMSO), chloroform, and a series of alcohols. McMorrow and Lotshaw have previously presented a detailed description of the transient birefringence of acetonitrile.[5] The improved time resolution used here reveals a distinctive intramolecular vibrational contribution in addition to the intermolecular signal.

In the figures presented below, we have fitted the signal with Eqs. (5.6a) and (5.6b) which assume an impulsive probe. Although the probe pulse profile is assumed to be impulsive, the deconvolution technique described in Sec. VII was used to eliminate the pump pulse profile and electronic response from the raw signal to obtain the nuclear response function. In order to compare the low-frequency distributions of different liquids and also to provide representative data for future studies, we have made fits by introducing a functional form for the spectral density

$$\chi_{ZZZZ}(t) - \chi_{YYZZ}(t) = \theta(t) \int_0^\infty d\omega\, \rho_{\rm bir}(\omega) \sin \omega t$$

with the spectral density

$$\rho_{\rm bir}(\omega) \propto \omega \exp(-\omega/\omega_c). \tag{8.1}$$

Here $\omega_c$ denotes a characteristic constant representing the frequency at the maximum of Eq. (8.1). This form of the spectral density is called as Ohmic spectrum in the paper of Legget *et al.*[51] Taking $\omega_c$ as a parameter, we fit the $\mathrm{Im}[\chi(\omega)]$'s with Eq. (8.1). The fitted parameters are listed in Table I. We hope this data set will be useful for further investigations and comparisons with independent studies of these liquids.

The signal for pure acetonitrile is shown in Fig. 2(a). The initial peak is the electronic contribution, and follows the instrument function almost exactly. The oscillatory behavior results from an intramolecular vibrational mode whose frequency is 380 $cm^{-1}$. The dotted line in Fig. 2(a) is the signal calculated using the procedure obtained above [see Eq. (5.6b)]. In order to compare the two signals, we normalize the peaks at $t=0$ for both the transient birefringence and simulated stimulated-Raman scattering signals. The relative contribution of the nuclear response is much greater in the transient birefringence signal than in the coherent Raman scattering. A semilogarithmic plot of the acetonitrile signal shows strong nonexponential behavior for times less than 2 ps. Thus it is difficult to extract the reorientational time constant from our signal. The frequency distribution of both the inter- and intramolecular modes can be directly seen in Fig. 2(b). The sharp peak around 15 $cm^{-1}$ results from the slowly decaying feature in the time-domain signal. The width of the low-frequency distribution from 0 to 170 $cm^{-1}$ is estimated to be about 80 $cm^{-1}$. The ratio between the areas of low-frequency modes (0 to 170 $cm^{-1}$) to the 380 $cm^{-1}$ intramolecular mode is about 7:1.

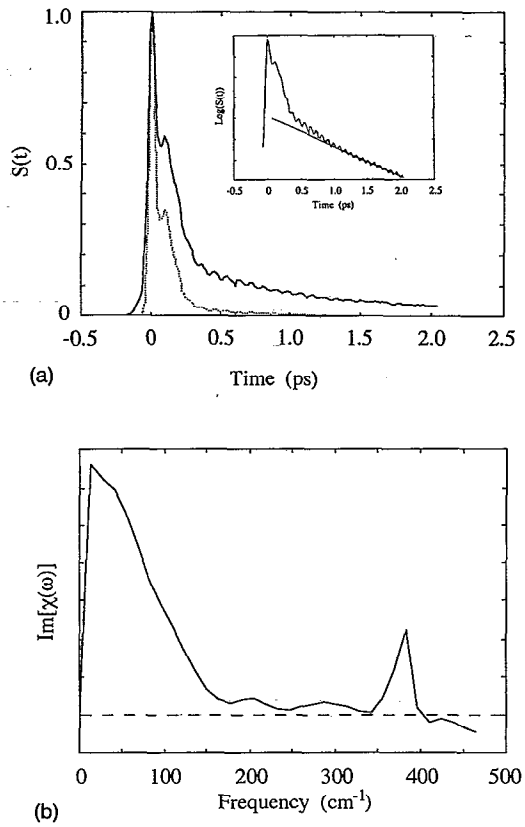


FIG. 2. (a) Experimental off-resonant transient birefringence (solid line) and simulated coherent Raman scattering (dotted line) signals for $CH_3CN$. Here, the maxima of the two signals at $t=0$ are matched. A semilogarithmic plot of the off-resonant transient birefringence signal of $CH_3CN$ is drawn in the inset. (b) Imaginary part of $\chi(\omega)$ for $CH_3CN$.

The transient birefringence signal of pure DMSO is shown in Fig. 3(a). The dotted line is again the simulated stimulated-Raman scattering signal. The peaks of the two signals are matched. The nuclear contribution is sufficiently small compared to the electronic contribution, that it is difficult to discern the nuclear response in the coherent Raman signal. The coherent Raman signal is roughly the square of the transient birefringence signal [see Eq. (5.6c)]. The inset in Fig. 3(a) is coherent Raman signal enlarged 1000 times. This signal is always positive. In Fig. 3(b) the imaginary part of $\chi(\omega)$ shows three groups of

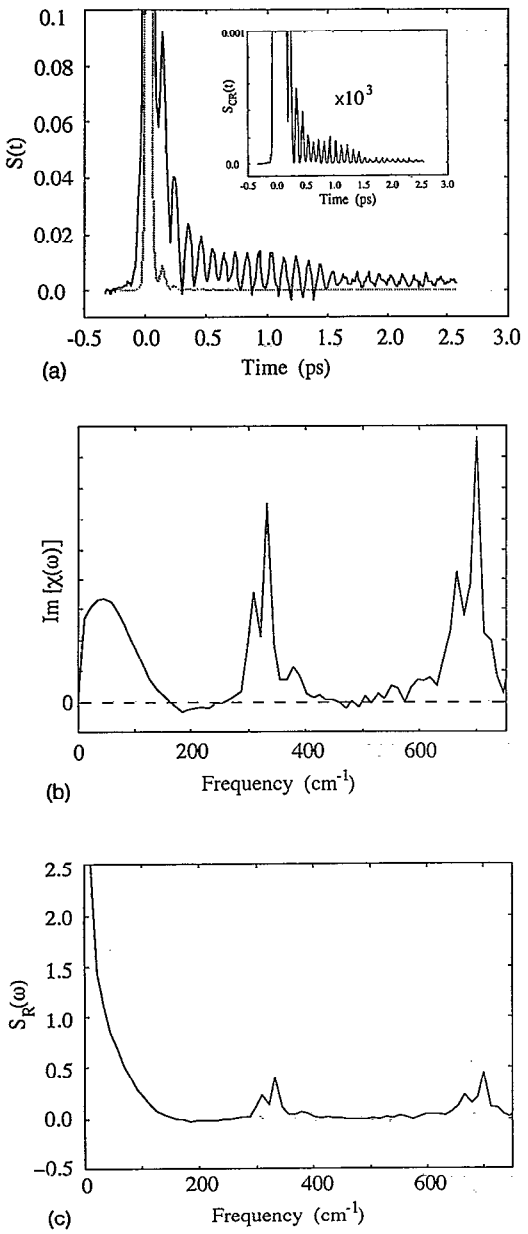


FIG. 3. (a) Experimental off-resonant transient birefringence (solid line) and simulated coherent Raman scattering (dotted line) signals for DMSO. The maxima of the two signals at $t=0$ are matched. The inset shows the coherent Raman scattering signal enlarged by 1000 times. (b) Imaginary part of $\chi(\omega)$ for DMSO. (c) Simulated spontaneous Raman spectrum of DMSO [see Eq. (5.8)].

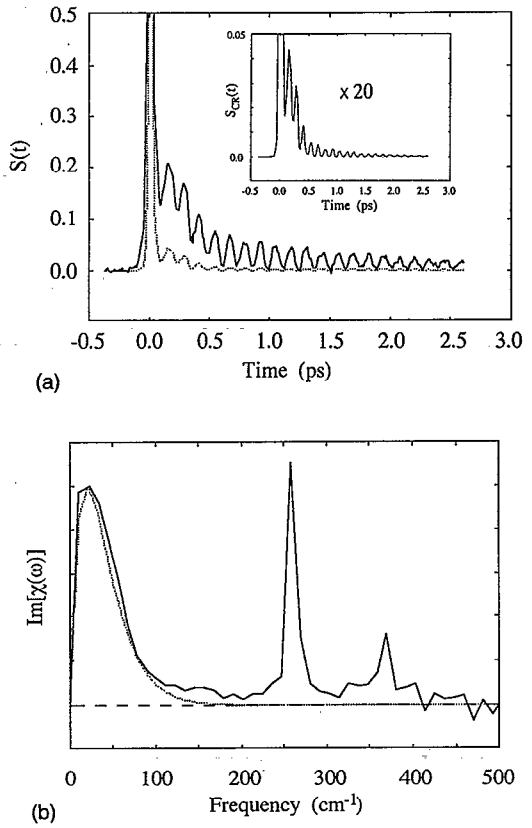


FIG. 4. (a) Experimental off-resonant transient birefringence (solid line) and simulated coherent Raman scattering (dotted line) signals of $CHCl_3$. The inset shows the coherent Raman scattering signal enlarged by 20 times. The maxima of the two signals at $t=0$ are matched. (b) Imaginary part of $\chi(\omega)$ of $CHCl_3$. The dotted line is the fitted spectral density with Eq. (8.1).

vibrational modes. Within our resolution of 11 $cm^{-1}$, the frequencies of intramolecular modes are estimated as 310, 330, 380, 665, and 700 $cm^{-1}$. The ratio of areas of the three groups of vibrational modes is 1.5 (30 $cm^{-1}$): 1 (310, 330, 380 $cm^{-1}$): 1.5 (665, 700 $cm^{-1}$). The same five intramolecular vibrational modes are also observed in the depolarized Raman spectrum measured by Horrocks and Cotton.[52] The simulated depolarized Raman spectrum of pure DMSO liquid is shown in Fig. 3(c). The relative magnitudes of each intramolecular vibrational mode contribution match precisely with the measured Raman peaks. Thus transient birefringence measurements should have value for quantitative analysis of the single and collective molecular polarizabilities. Because of the correction factor, $[1-\exp(-\hbar\omega/k_BT)]^{-1}$ in the depolarized Raman spectrum, the low frequency region in depolarized Rayleigh wing spectroscopy is greatly suppressed compared to the imaginary part of $\chi(\omega)$ shown in Fig. 3(b). Transient birefringence thus provides a clear spectrum of the low frequency features. The width of the low-frequency lobe running from 0 to 180 $cm^{-1}$ is about 90 $cm^{-1}$. The width and shape of low-frequency distribution in DMSO is almost identical to that of acetonitrile [compare with Fig. 2(b)].

In Fig. 4(a) we show the transient birefringence signal of pure chloroform. The simulated stimulated-Raman scattering signal is drawn as a dotted line in the same figure. The two distinctive vibrational modes with frequencies are 260 and 370 $cm^{-1}$ are identified in Fig. 4(b), which shows the imaginary part of $\chi(\omega)$. The width of the low-frequency feature from 0 to 110 $cm^{-1}$ is about 55 $cm^{-1}$. The ratio of areas of the three regions is roughly 9 ($<100$ $cm^{-1}$): 3 (260 $cm^{-1}$): 1 (370 $cm^{-1}$), respectively.

The imaginary parts of the response functions of various alcohols are shown in Figs. 5(a) and 5(b). Because our spectra are rather noisy in the high-frequency region

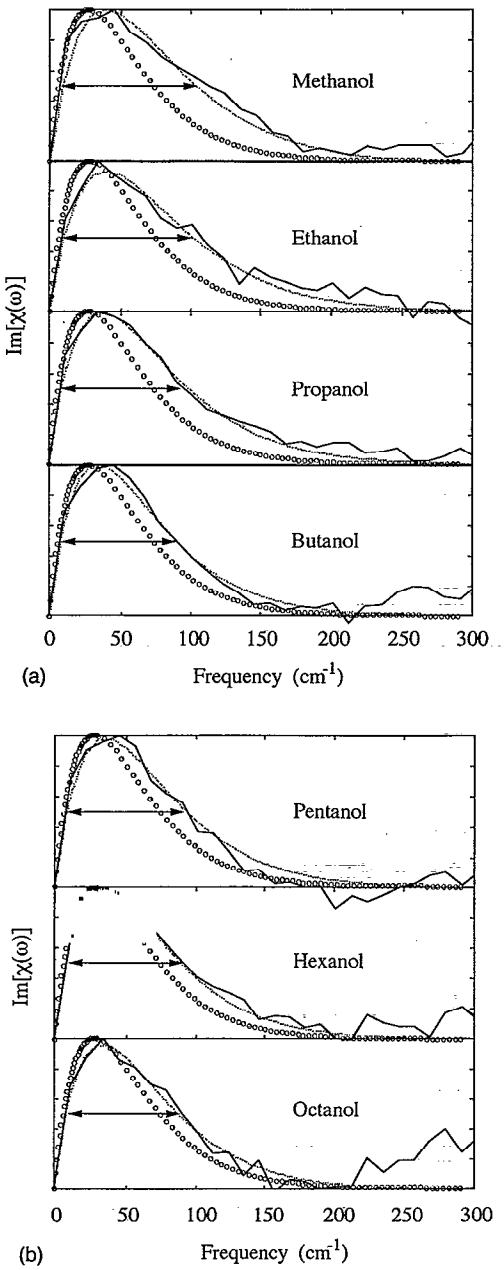


FIG. 5. (a) The imaginary parts of $\chi(\omega)$'s of $CH_3(CH_2)_nOH$ ($n$=0, 1, 2, and 3) are shown. The dotted lines are the best fits with Eq. (8.1). The circles are the experimental data points calculated from the depolarized Rayleigh scattering signal with the parameters obtained by Benassi *et al.* (Ref. 50). (b) The same as (a) but $n$=4, 5, and 7.

($>300$ cm$^{-1}$), we focus on the low-frequency region. The shapes of these spectra are very similar to each other, although the methanol spectrum is slightly broader than the longer-chain alcohols. The maxima of the spectra are all around 40 cm$^{-1}$. The methanol spectrum shows a shoulder around 100 cm$^{-1}$. The slowly decaying component in the optical Kerr signal is generally assigned to a single molecular reorientational motion. Our data extends to only 2.5 ps making it difficult to extract the reorientational dynamics accurately. In general we would expect multiexponential behavior for such asymmetric molecules.

The low-frequency ($<300$ cm$^{-1}$) distributions shown in Figs. 2(b), 3(b), 4(b), 5(a), and 5(b) are the spectral densities which are needed to specify the time scale of the molecular motions of the corresponding liquid.

## IX. DISCUSSION

Despite the vast literature on vibrational (such as infrared and Raman) spectroscopies,[53] the molecular aspects of the low-frequency modes involving more than a few molecules observed in the far IR and Rayleigh-wing spectroscopies are poorly understood. Most existing theoretical models are based on hydrodynamic or phenomenological descriptions of the dynamical motions. A lack of understanding of the low frequency collective molecular motions partly originates from the difficulty of experimental measurement of these modes via frequency-domain spectroscopies. Although, in Sec. V B, we showed the direct relationship between off-resonant transient birefringence and spontaneous Raman spectroscopy, we should consider these two experimental techniques as complimentary tools for studying molecular dynamics in condensed phases. We first discuss the vibrational excitation process in the off-resonant transient birefringence by considering the impulsive force created by the off-resonant pump field. The intermolecular vibrational contributions observed in the imaginary parts of $\chi(\omega)$ of various liquids are then discussed. Using Eqs. (5.6) and (5.8), we numerically calculate the depolarized forward coherent Raman scattering signal and spontaneous Raman spectra to demonstrate the relative relationships among different experimental techniques.

From Eqs. (3.3) and (3.4), the impulsive nature of the external perturbation onto the system can be understood by considering the associated force exerted on the $j$th degree of freedom $F_j(t)=|E_1(t)|^2\hat{e}_1\hat{e}_1:\partial\tilde{\alpha}(\omega)/\partial q_j$. It should be emphasized that $\tilde{\alpha}(\omega_1)$ represents the collective polarizability of the sample, not just a sum of single molecular polarizabilities. Thus vibrational excitations of both inter- and intramolecular modes may be obtained through this process.

In the case of a spherical molecule, the time-dependent single molecular polarizability does not depend on the molecular orientation, that is to say the molecular polarizability is isotropic. Thus the depolarized component of the Raman signal of a simple liquid, e.g., argon, is expected to vanish. However, a depolarized, collision-induced, component which is attributed to the dipole–induced-dipole interaction, and which is forbidden for the isolated atom is observed in this liquid. Geiger and Ladanyi showed the importance of contributions from higher order interaction-induced effects in the Rayleigh scattering of $CS_2$ liquid.[30(a)] They also compared the calculated stimulated-Raman scattering and off-resonant transient birefringence[30(b)] with the corresponding signals measured by Ruhman *et al.*[6] and Kalpouzos *et al.*,[2] respectively. The close agreement observed in both cases suggests a crucial contribution from higher-order interaction-induced effects in liquid $CS_2$. In order to describe the dynamical aspects of the collective polarizability, it is usually separated into the collective ori-

entational and interaction induced terms. Then, by considering these two terms separately the molecular aspects of the dynamical motions have been studied by means of computer simulations. By Fourier transforming $\chi(t)$ [Eq. 3.13)] we obtain a characteristic power spectrum of the liquid related to the response function associated with the polarizability $\alpha$. Since the collective (intermolecular) polarizability generally involves many-body dynamics, it is difficult to calculate the transient birefringence rigorously without invoking simplifying assumptions. Eq. (4.20) suggests the interpretation of these power spectra in terms of the dynamics of intermolecular vibrational modes, which represent the collective motions of the liquid [see Eqs. (4.7)]. Further, these intermolecular vibrational modes are assumed to obey stochastic Brownian dynamics [Eq. (4.17)].[5,29] The collective orientational contributions may be described by corresponding intermolecular vibrational modes. Obviously, nuclear motions in liquids have large amplitudes and we do not expect the normal mode picture to hold for long times. We found that the dynamical responses of various liquids given in the previous section show very fast decay patterns, i.e., times less than 1 ps. Therefore, we might expect the short time behavior of liquids may be sufficient to describe the observed ultrafast responses. As discussed below Eq. (4.8), the diffusive reorientational contribution was introduced to describe the long-time tail of the signal. In most of the off-resonant transient birefringence signals we shall present, this portion of the signal is very small in magnitude. We expect, therefore, comparatively little error to be introduced in the description of the short time dynamics by the approximation made in Eq. (4.8). However, the dynamics of the single molecular reorientational motion will be found to be important in the description of the intramolecular vibrational dynamics, since the purely vibrational response function is multiplied by the single reorientational contribution. By measuring the isotropic part of the response function [see Eq. (4.12a)], the vibrational relaxation may be observed without a contribution from reorientational motion. Finally the molecular reorientational dynamics can be extracted without ambiguity from the comparison of the isotropic and anisotropic measurements.

In Figs. 2(b) and 3(b), we observe that the low-frequency power spectra of acetonitrile and DMSO are very similar. On the other hand, the intermolecular vibrational frequency distribution of chloroform is peaked at lower frequency and is narrower than those of acetonitrile and DMSO. It should be noted that the spectra shown here are obtained by using the numerical deconvolution methods discussed in Sec. VII. Thus each spectrum contains all nuclear responses regardless of any dynamical model. In the present experiment, the signals were measured only up to 2 or 2.5 ps and so not attempted to separate the contributions from the diffusive reorientational motion and intermolecular vibrational motion. However, it would be reasonable to consider that the higher frequency ($>10\ \mathrm{cm}^{-1}$) portion of the spectra represents largely contributions from the intermolecular vibrational motions. At our present stage of understanding a detailed study of the intermolecular vibrational dynamics of these dipolar liquids via molecular dynamics simulation appears necessary to interpret the molecular nature of the response. A careful study of the power spectrum of small clusters and its size convergence to the bulk may provide a useful means for determining the nature of the collective modes.[54,55]

From Fig. 5, we note that the spectral width of the imaginary parts of $\chi(\omega)$ of the shorter chain alcohols is broader than that of the longer-chain alcohols. If the reorientational motions are involved, the moment of inertia should play a role in determining the spectra. Although the moment of inertia increases as the chain length increases, we observe a limiting behavior in the widths and peaks of $\mathrm{Im}[\chi(\omega)]$ of long-chain alcohols. Since it is certainly a crude assumption that the long-chain alcohols are linear sticklike molecules we expect that intramolecular dynamics, for example rotational isomerization about the dihedral axes, could be involved in the liquid responses. Even though the number of the intramolecular degrees of freedom increases with respect to the chain length, we do not observe any significant changes in the spectra resulting from these additional dynamical motions. We also observe that the peak of $\mathrm{Im}[\chi(\omega)]$ of methanol is around 40 $\mathrm{cm}^{-1}$ whereas that of octanol is around 35 $\mathrm{cm}^{-1}$. The contributions from rotational degrees of freedom are very similar, for example, in butanol and octanol. Overall, the difference in the $\mathrm{Im}[\chi(\omega)]$'s for the various alcohols is very small in comparison to the differences of moments of inertia and total masses. Benassi *et al.* measured the depolarized and polarized Rayleigh scattering signals of alcohols, $CH_3(CH_2)_nOH$ with $n=0$–4,[56] over the frequency range from 0 to 70 $\mathrm{cm}^{-1}$. They found that the high frequency parts (from 10 to 70 $\mathrm{cm}^{-1}$) of the depolarized-Rayleigh wing spectra of various alcohols are almost identical and decay as an exponential, $S_R(\omega) \propto \exp(-\omega/\Delta)$ with $\Delta=29$ $\mathrm{cm}^{-1}$. In Figs. 5(a) and 5(b), we show the calculated spectral density by using this expression multiplied by the correction factor $[1-\exp(-\hbar\omega/kT)]$. We find good agreement up to 70 $\mathrm{cm}^{-1}$; after this our data and the extrapolated curves of Benassi *et al.* diverge. However, we are not sure whether extrapolation beyond 70 $\mathrm{cm}^{-1}$ is warranted and it is clear that depolarized Rayleigh scattering measurements are very difficult in the intermediate frequency region (from 50 to 500 $\mathrm{cm}^{-1}$) because of the small signal to noise ratio. On the other hand, time-resolved measurements such as off-resonant transient birefringence show great sensitivity in this freqency region. By measuring decays out to longer times—note our measurements are usually limited to 2.5 ps—we can increase the resolution of the low frequency region ($<50\ \mathrm{cm}^{-1}$). Finally we also observed that the long-time decays in the various liquid alcohols did not show exponential behavior in the time range accessed.

Now, using the model-independent relationships between various off-resonant spectroscopies discussed in Sec. V, we compare the off-resonant transient birefringence and coherent Raman scattering measurements. Coherent Raman scattering spectroscopy involves a second pump field propagating differently from the other pump field. Also,

since the polarization directions of both the three pulses (two pump and one probe pulses) and the detection can be arbitrarily controlled, the coherent Raman scattering techniques can measure various tensorial components of the total (both electronic and nuclear) response.[6(c)] If one wants to measure the pure nuclear response, it would be necessary to deconvolute the laser intensity profile from the raw signal [see Eqs. (5.5) and (5.6)]. Because the measured signal is linearly proportional to the response function in the case of the off-resonant transient birefringence, it is always possible to separate the nuclear contributions from the total response function (see Sec. VII). In contrast, the coherent Raman scattering signal (for example, the depolarized forward coherent Raman scattering signal) is proportional to the square of the convolution integral [see Eqs. (5.6)], which makes it difficult to extract the nuclear response without making a fit to the whole signal with a suitable model.

We now turn to the vibrational spectral density defined in Eq. (4.21), and to its relationship with the spin-Boson model.[51,57] The vibrational spectral density is equal to $\mathrm{Im}[\chi(\omega)]$ obtained by using the Fourier transform technique used in the present paper. The way we choose to parametrize it depends on the physical picture we adopt. One possibility is to think of the liquid as a collection of a large number of normal modes (which may be applicable for short times). We then use the expansion [Eq. (4.21)] and write

$$\rho_{\mathrm{bir}}(\omega)=\sum_j \frac{c_j}{M_j\omega_j}\delta(\omega-\omega_j) \tag{9.1}$$

with

$$c_j\equiv\left[\left(\frac{\partial\tilde{\alpha}}{\partial Q_j}\right)_{y_0}\otimes\left(\frac{\partial\tilde{\alpha}}{\partial Q_j}\right)_{y_0}\right]_{ZZZZ} -\left[\left(\frac{\partial\tilde{\alpha}}{\partial Q_j}\right)_{y_0}\otimes\left(\frac{\partial\tilde{\alpha}}{\partial Q_j}\right)_{y_0}\right]_{YYZZ}. \tag{9.2}$$

Here it should be noted that the above definition of the spectral density is obtained when $\gamma_j=0$ in Eq. (4.19), that is to say, the renormalized frequency $\Omega_j=\omega_j$. By parametrizing $\rho(\omega)$, we make assumptions about the density of modes, weighted by their coupling to the radiation field (through the polarizability). In this picture, the modes are treated as harmonic oscillators with no damping. In case of the associating liquids, i.e., water, and the short-chain alcohols, the short-time dynamics can be well approximated by a harmonic description with a corresponding frequency distribution. In this case the intermolecular vibrational coordinates are directly related to the liquid phonons. To get analytic expressions, one may model the spectral densitiy in various ways, e.g., Ohmic, Drude, super-Ohmic, and so on.[51] For example, a Drude spectral density eventually gives an exponentially decaying function when transformed to the time domain. Alternatively, we may choose to look at a few collective coordinates and model them using a reduced equation, e.g., the generalized Langevin equation,[48,58–62] with a time-dependent memory function. We then parametrize $\mathrm{Im}\,\chi(\omega)$ in terms of a frequency-dependent friction $\gamma(\omega)$.

The two parametrization schemes are completely equivalent since by starting with a model of a few primary oscillators coupled to a harmonic bath we can either find the global normal modes of the coupled system, or derive a generalized Langevin equation. The choice, therefore, depends entirely on the physical picture we wish to adopt. $\gamma(\omega)$ can be calculated by computer simulations or by assuming some simplified models, such as exponential or Gaussian. However, the merit of such simple models is not clear, since the time-dependent memory functions calculated from MD simulations are quite complex.[63,64]

The present analysis is for electronically off-resonant spectroscopies. For resonant conditions we need to consider the coupling of the electronic two level system to the bath. In this case we can adopt the spin-Boson Hamiltonian which has been quite extensively used to understand the influence of the dissipative bath on a spin system,[57,65] electron transfer,[66–68] electronically excited molecules,[69] and spectroscopic line broadenings.[70] A rigorous connection between reaction rates and the nonlinear optical response for this model has been established.[55] Basically, the associated dynamical variables are linearly coupled to the harmonic undamped oscillator bath. Because of its simplicity in describing the complicated many-body aspect of a general bath, analytic expressions for interesting quantities can be obtained. The key quantity specifying the fluctuation-dissipation relationship between the bath and dynamical variable is the spectral density that is in general determined by both the frequency distribution and the coupling constants of each harmonic bath mode. For example, Pollak[71] showed that the Grote–Hynes expression[72] of the transmission coefficient based on the generalized Langevin equation of an inverted harmonic potential surface can be derived by using a Hamiltonian of a unstable harmonic mode linearly coupled to the harmonic oscillator bath. Using the path-integral technique, the multidimensional tunneling problem has also been extensively studied.[51,57,73] Many applications of the harmonic bath model have proved the usefulness of this simple model to understand the role of dissipative interaction and to provide a guide for further developments theoretically as well as experimentally. The optical nonlinear response function for the spin Boson model to arbitrary order in the radiation field and including an arbitrary (non-Condon) dependence of the transition dipole on nuclear coordinates has been calculated by Tanimura and Mukamel using path integral techniques.[70] The resulting expression applies to resonant as well as off resonant conditions, and in the off-resonant limit it agrees with our present results.

Off-resonant measurements can always be parametrized in terms of a multimode harmonic model and therefore do not provide a critical test for its physical applicability. However, since the oscillator picture has a unique prediction with regard to the resonant behavior and regarding the temperature dependence of the optical response, it is possible to use such measurements to test the

model. Such tests have not been made so far. The following example illustrates the importance of carrying out resonant measurements. Suppose we have an inhomogeneous distribution of oscillators

$$\rho(\omega)=\int d\Gamma\ \rho_0(\omega,\Gamma)P(\Gamma). \tag{9.3}$$

We assume that the liquid has domains with a slow interconversion rate between them. $\Gamma$ can stand for $Q_0$ (a specific liquid configuration) or any other parameter that defines the domain. One can envision an infinite number of choices of $\rho_0(\omega)$ and $P(\Gamma)$ that will yield the same whole spectral density, $\rho(\omega)$. Nevertheless, the off resonant response will depend solely on $\rho$. Resonant measurements such as photon echoes will however be very different for these various choices, which represent a completely different physical picture. Fried and Mukamel have developed the inhomogeneous cumulant expansion which addresses this problem.[62] Bearing this problem in mind, we suggest that the spectral density obtained from the transient birefringence signal could serve as an experimental method to determine the spectral distribution (i.e., time scale distribution) of the harmonic bath [see Eq. (4.21)]. We recall that the coupling constants ($c_\alpha$) in the transient birefringence depend on the nuclear cordinate-dependent Raman polarizability. In general, the coupling constants may have a strong dependence on the relevant dynamical variables such as polarizability in Raman spectroscopy, dipole moment in IR spectroscopy, macroscopic solvent polarization, and so on. The observation of Keyes and Seely,[74] that the light scattering spectrum of a simple liquid is very similar to the instantaneous normal mode spectrum, suggests that the coupling constants which are ingredients in the spectral density are likely to be independent on the frequency of the harmonic mode. Thus, the frequency distribution of the harmonic modes seems to be the major factor in the spectral density profile. The molecular system studied is very simple and contains no rotational degrees of freedom, Buchner *et al.*'s work[75] on the instantaneous normal mode analysis of a diatomic molecular liquid again supports this conjecture.

## X. SUMMARY

In the present paper, we derived a master equation for off-resonant pump–probe spectroscopies employing polarized fields. For far off-resonant excitation, the excited state density matrix element is effectively decoupled, since the imaginary part of the linear susceptibility is negligibly small. Thus, the effective Hamiltonian is simply obtained by adding a driving force $|E_1(t)|^2\hat{e}_1\hat{e}_1:\tilde{\alpha}(\omega_1)$ to the adiabatic ground state Hamiltonian. When the pump field is weak, we solve the master equation perturbatively to obtain Eq. (3.10). The third-order macroscopic polarization created by the external pump field was determined by the expectation value of the molecular polarizability tensor. The off-resonant birefringence signal is finally given by the convolution of the response function of the molecular polarizability tensors and the external fields [Eq. (3.12)].

A comparison of the heterodyne- and the homodyne-detected birefringence with the coherent Raman signal was presented. By expanding the polarizability with respect to the corresponding coordinates and assuming Brownian motion for the vibrational coordinate response functions, we obtained the signal as a sum of the correlation functions of the Brownian oscillators.

The relationship between the off-resonant birefringence signal and the spontaneous Raman signal was established by using the fluctuation-dissipation theorem which relates the response function of the polarizability to the correlation function of the polarizability by Eq. (5.7).

Experimental measurements of off-resonant transient birefringence of acetonitrile, chloroform, DMSO, and a series of alcohols were presented and compared in the frequency domain. Except for a weak trend of redshift from short- to long-chain alcohols, the overall shapes of the spectral densities are remarkably similar. Also, we observed distinctive intramolecular vibrational beats in acetonitrile, chloroform, and DMSO. Low-frequency distributions were adequately represented by the function $\omega\times\exp(-\omega/\omega_c)$. When the coupling constants are independent on intermolecular vibrational frequencies, we suggest that the crucial input for spin-Boson model can be obtained by the off-resonant transient birefringence, and thus the results presented here may have some value for predicting various dynamical phenomena in the same liquids.

## ACKNOWLEDGMENTS

This work was supported by the National Science Foundation. We thank Mr. Yiwei Jia for providing us a fitting program and helpful discussions.

## APPENDIX A

In this Appendix, we consider a single molecular response function for off-resonant birefringence. Let **u** be a unit vector which lies along the symmetry axes of a symmetric top molecule. In this appendix, we treat the rotational motion classically. The polarizability tensor can be in this case expressed as

$$\alpha_{ij}=\alpha_\parallel\ u_iu_j+\alpha_\perp\ (\delta_{ij}-u_iu_j), \tag{A1}$$

where $u_i$ is the $i$th component of the unit vector **u**. $\alpha_\parallel$ and $\alpha_\perp$ designate the polarizabilities along the symmetry axis and along any axis perpendicular to **u**. By defining

$$\alpha\equiv\tfrac{1}{3}(\alpha_\parallel+2\alpha_\perp)\ \text{and}\ \beta\equiv(\alpha_\parallel-\alpha_\perp), \tag{A2}$$

Eq. (A1) can be rewritten as

$$\alpha_{ij}=\alpha\delta_{ij}+\beta_{ij} \tag{A3}$$

with

$$\beta_{ij}=\beta(u_iu_j-\tfrac{1}{3}\delta_{ij}). \tag{A4}$$

Here we are using the Einstein convention stipulating that repeated indices be summed (i.e., $\alpha_{ii}=\alpha_{11}+\alpha_{22}+\alpha_{33}$, $\delta_{ii}=\delta_{11}+\delta_{22}+\delta_{33}=3$, $\delta_{ij}\delta_{ji}=3$ and so on). Since $\alpha\delta_{ij}$ is not dependent of **u**, this does not change as the molecule

rotates. $\beta_{ij}$ on the other hand, depends on the molecular reorientation. It should be noted that the polarizability tensor $\alpha_{ij}$ is symmetric in the indices $i$, $j$ (i.e., $\alpha_{ij}=\alpha_{ji}$ and $\beta_{ij}=\beta_{ji}$). For isotropic media, the average of $\beta_{ij}$ over the initial orientational distribution is zero, and therefore $\langle\alpha_{ij}\rangle = \alpha\delta_{ij}$. This is crucial in comparing the off-resonant birefringence with the coherent or spontaneous Raman scatterings. If the media is initially isotropic, the depolarized (VH) component of the coherent and spontaneous light scatterings contains the same information with the anisotropic signal of off-resonant birefringence [compare Eq. (A11) and (B4)].

A single molecular contribution to the polarizability response function for off-resonant birefringence is then

$$\chi_{\beta\beta\alpha\alpha}(t)=\left\langle\frac{i}{\hbar}[\alpha_{\beta\beta}(t),\alpha_{\alpha\alpha}(0)]\right\rangle$$
$$=N_{ij}^{\beta\beta}\left\langle\frac{i}{\hbar}[\alpha_{ij}(t),\alpha_{kl}(0)]\right\rangle N_{kl}^{\alpha\alpha} \quad \text{(A5)}$$

with

$$N_{ij}^{\beta\beta}=(n_\beta)_i(n_\beta)_j \text{ and } N_{kl}^{\alpha\alpha}=(n_\alpha)_k(n_\alpha)_l, \quad \text{(A6)}$$

where subscripts $\alpha$ and $\beta$ represent the polarization direction of the pump and probe (also local oscillator) beams respectively, and $(n_\alpha)_i$ denotes an $i$th component of the unit vector which lies along the laboratory $\alpha$ axis.

Inserting Eq. (A3) into Eq. (A5) and using the rotational invariant property of $\alpha\delta_{ij}$ and $\langle\beta_{ij}\rangle=0$ give (refer to Appendix 7.B in Ref. 47)

$$\left\langle\frac{i}{\hbar}[\alpha_{ij}(t),\alpha_{kl}(0)]\right\rangle$$
$$=\left\langle\frac{i}{\hbar}[\alpha(t),\alpha(0)]\right\rangle\delta_{ij}\delta_{kl}+\left\langle\frac{i}{\hbar}[\beta_{ij}(t),\beta_{kl}(0)]\right\rangle$$
$$=\left\langle\frac{i}{\hbar}[\alpha(t),\alpha(0)]\right\rangle\delta_{ij}\delta_{kl}+\frac{1}{15}\left\langle\frac{i}{\hbar}[\beta(t),\beta(0)]\right\rangle$$
$$\times\langle P_2[\mathbf{u}(0)\cdot\mathbf{u}(t)]\rangle[\delta_{ik}\delta_{jl}+\delta_{il}\delta_{jk}-\tfrac{2}{3}\delta_{ij}\delta_{kl}], \quad \text{(A7)}$$

where $P_2(x)=3x^2/2-1/2$. By substituting Eq. (A7) into Eq. (A5), the response function is then written as

$$\chi_{\beta\beta\alpha\alpha}(t)=\left\langle\frac{i}{\hbar}[\alpha(t),\alpha(0)]\right\rangle+\frac{4}{45}P_2(\mathbf{n}_\beta\cdot\mathbf{n}_\alpha)$$
$$\times\left\langle\frac{i}{\hbar}[\beta(t),\beta(0)]\right\rangle\langle P_2[\mathbf{u}(0)\cdot\mathbf{u}(t)]\rangle. \quad \text{(A8)}$$

For example, if $\mathbf{n}_\alpha$ and $\mathbf{n}_\beta$ are parallel,

$$\chi_{ZZZZ}(t)=\left\langle\frac{i}{\hbar}[\alpha(t),\alpha(0)]\right\rangle+\frac{4}{45}\left\langle\frac{i}{\hbar}[\beta(t),\beta(0)]\right\rangle$$
$$\times\langle P_2[\mathbf{u}(0)\cdot\mathbf{u}(t)]\rangle. \quad \text{(A9)}$$

On the other hand, if $\mathbf{n}_\alpha$ and $\mathbf{n}_\beta$ are perpendicular, we have

$$\chi_{YYZZ}(t)=\left\langle\frac{i}{\hbar}[\alpha(t),\alpha(0)]\right\rangle-\frac{2}{45}\left\langle\frac{i}{\hbar}[\beta(t),\beta(0)]\right\rangle$$
$$\times\langle P_2[\mathbf{u}(0)\cdot\mathbf{u}(t)]\rangle. \quad \text{(A10)}$$

As will be discussed later, the conventional off-resonant birefringence measurement is related to

$$\chi_{ZZZZ}(t)-\chi_{YYZZ}(t)=\frac{2}{15}\left\langle\frac{i}{\hbar}[\beta(t),\beta(0)]\right\rangle$$
$$\times\langle P_2[\mathbf{u}(0)\cdot\mathbf{u}(t)]\rangle. \quad \text{(A11)}$$

Equation (A11) is proportional to the anisotropic part of the response function [see Eq. (4.12b)]. The isotropic part is measured by

$$\chi_{ZZZZ}(t)+2\chi_{YYZZ}(t)=3\left\langle\frac{i}{\hbar}[\alpha(t),\alpha(0)]\right\rangle \quad \text{(A12)}$$

which is corresponding to the isotropic part of the response function defined in Eq. (4.12a).

## APPENDIX B

For coherent Raman scattering (or impulsive stimulated Raman scattering) with zero wave vector, the corresponding response functions are of the form $\chi_{\alpha\beta\alpha\beta}$, whereas the response functions for off-resonant birefringence are $\chi_{\beta\beta\alpha\alpha}$. The response function for forward ($\mathbf{k}=0$) coherent Raman scattering is then

$$\chi_{\beta\alpha\beta\alpha}(t)=\left\langle\frac{i}{\hbar}[\alpha_{\beta\alpha}(t),\alpha_{\beta\alpha}(0)]\right\rangle$$
$$=N_{ij}^{\beta\alpha}\left\langle\frac{i}{\hbar}[\alpha_{ij}(t),\alpha_{kl}(0)]\right\rangle N_{kl}^{\beta\alpha} \quad \text{(B1)}$$

with

$$N_{ij}^{\beta\alpha}=(n_\beta)_i(n_\alpha)_j \text{ and } N_{kl}^{\beta\alpha}=(n_\beta)_k(n_\alpha)_l. \quad \text{(B2)}$$

The difference between Eqs. (A5) and (B1) is the projections of the molecular polarizability onto the polarization directions of the external fields. Inserting Eq. (A7) into Eq. (B1) gives

$$\chi_{\beta\alpha\beta\alpha}(t)=\left\langle\frac{i}{\hbar}[\alpha(t),\alpha(0)]\right\rangle(\mathbf{n}_\beta\cdot\mathbf{n}_\alpha)^2$$
$$+\frac{1}{15}\left\langle\frac{i}{\hbar}[\beta(t),\beta(0)]\right\rangle[1+\tfrac{1}{3}(\mathbf{n}_\beta\cdot\mathbf{n}_\alpha)^2]$$
$$\times\langle P_2[\mathbf{u}(0)\cdot\mathbf{u}(t)]\rangle. \quad \text{(B3)}$$

For $n_\alpha\| n_\beta$, the corresponding response function for the impulsive stimulated Raman scattering is $\chi_{ZZZZ}(t)$, which was given in Eq. (A9). For $\mathbf{n}_\alpha\perp\mathbf{n}_\beta$,

$$\chi_{YZYZ}(t)=\frac{1}{15}\left\langle\frac{i}{\hbar}[\beta(t),\beta(0)]\right\rangle\langle P_2[\mathbf{u}(0)\cdot\mathbf{u}(t)]\rangle. \quad \text{(B4)}$$

Clearly, the depolarized (VH) component, i.e., $\chi_{YZYZ}(t)$ of the forward impulsive light scattering is iden-

tical to the anisotropic measurement of the off-resonant birefringence [compare Eqs. (A11) and (B4)],

$$\chi_{ZZZZ}(t)-\chi_{YYZZ}(t)=2\chi_{YZYZ}(t). \tag{B5}$$


[1] E. P. Ippen and C. V. Shank, Appl. Phys. Lett. **26**, 92 (1975).
[2] (a) C. Kalpouzos, W. T. Lotshaw, D. McMorrow, and G. A. Kenney-Wallace, J. Phys. Chem. **91**, 2028 (1987); (b) D. McMorrow, W. T. Lotshaw, and G. A. Kenney-Wallace, IEEE J. Quantum Electron. **QE-24**, 443 (1988); (c) W. T. Lotshaw, D. McMorrow, C. Kalpouzos, and G. A. Kenney-Wallace, Chem. Phys. Lett. **137**, 323 (1987).
[3] B. I. Greene and R. C. Farrow, Chem. Phys. Lett. **98**, 273 (1983); B. I. Green, P. A. Fleury, H. L. Carter, and R. C. Farrow, Phys. Rev. A **29**, 271 (1984).
[4] T. Hattori and T. Kobayashi, J. Chem. Phys. **94**, 3332 (1991).
[5] D. McMorrow and W. T. Lotshaw, J. Phys. Chem. **95**, 10395 (1991).
[6] (a) S. Ruhman, A. G. Joly, and K. A. Nelson, J. Chem. Phys. **86**, 6563 (1987); (b) S. Ruhman, L. R. Williams, A. G. Joly, B. Kohler, and K. A. Nelson, J. Phys. Chem. **91**, 2237 (1987); (c) S. Ruhman, A. G. Joly, and K. A. Nelson, IEEE J. Quantum Electron. **QE-24**, 460 (1988); (d) S. Ruhman, B. Kohler, A. G. Joly, and K. A. Nelson, *ibid.* **QE-24**, 470 (1988).
[7] Y. X. Yan and K. A. Nelson, J. Chem. Phys. **87**, 6240, 6257 (1987).
[8] P. F. Barbara and W. Jarzeba, Adv. Photochem. **15**, 1 (1990).
[9] J. D. Simon, Acc. Chem. Res. **21**, 128 (1988).
[10] M. Maroncelli, J. Mol. Liq. (in press).
[11] E. W. Castner, Jr., M. Maroncelli, and G. R. Fleming, J. Chem. Phys. **86**, 1090 (1987).
[12] W. Jarzeba, G. C. Walker, A. E. Johnson, M. E. Kahlow, and P. F. Barbara, J. Phys. Chem. **92**, 7039 (1988).
[13] S. J. Rosenthal, X. Xie, M. Du, and G. R. Fleming, J. Chem. Phys. **95**, 4715 (1991).
[14] S. J. Rosenthal, N. F. Scherer, X. Xie, M. Cho, M. E. Schmidt, and G. R. Fleming, J. Chem. Phys. (submitted).
[15] R. F. Loring, Y. J. Yan, and S. Mukamel, J. Chem. Phys. **87**, 5840 (1987).
[16] Y. J. Yan and S. Mukamel, J. Chem. Phys. **94**, 997 (1991).
[17] D. Waldeck, A. J. Cross, Jr., D. B. McDonald, and G. R. Fleming, J. Chem. Phys. **74**, 3381 (1981).
[18] N. F. Scherer, L. D. Ziegler, and G. R. Fleming, J. Chem. Phys. **96**, 5544 (1992).
[19] D. S. Alavi, R. S. Hartman, and D. H. Waldeck, J. Chem. Phys. **94**, 4509 (1991).
[20] J. Chesnoy and A. Mokhtari, Phys. Rev. A **38**, 3566 (1988).
[21] J. A. Walmsley, M. Mitsunaga, and C. L. Tang, Phys. Rev. A **38**, 4681 (1988).
[22] M. D. Levenson and S. S. Kano, *Introduction to Nonlinear Laser Spectroscopy* (Academic, San Diego, 1988).
[23] M. Cho, G. R. Fleming, and S. Mukamel, J. Chem. Phys. **98**, 5314 (1993).
[24] (a) R. J. D. Miller, R. Casalegno, K. A. Nelson, and M. D. Fayer, Chem. Phys. **72**, 371 (1982); (b) K. A. Nelson, R. J. D. Miller, D. R. Lutz, and M. D. Fayer, J. Appl. Phys. **53**, 1144 (1982).
[25] M. D. Fayer, Ann. Rev. Phys. Chem. **33**, 63 (1982); J. T. Fourkas and M. D. Fayer, Acc. Chem. Res. **25**, 227 (1992).
[26] R. W. Hellwarth, Prog. Quantum Electron. **5**, 1 (1977).
[27] J. Etchepare, G. Grillon, J. P. Chambaret, G. Harmoniaux, and A. Orszag, Opt. Commun. **63**, 329 (1987).
[28] F. W. Deeg and M. D. Fayer, J. Chem. Phys. **91**, 2269 (1989).
[29] M. Cho, S. J. Rosenthal, N. F. Scherer, L. D. Ziegler, and G. R. Fleming, J. Chem. Phys. **96**, 5033 (1992).
[30] (a) L. C. Geiger and B. M. Ladanyi, J. Chem. Phys. **87**, 191 (1987); **89**, 6588 (1988); (b) Chem. Phys. Lett. **159**, 413 (1989).
[31] P. A. Madden and D. J. Tildesley, Mol. Phys. **49**, 193 (1983).
[32] P. A. Madden and Kivelson, Adv. Chem. Phys. **56**, 467 (1984).
[33] T. Keyes and B. M. Ladanyi, Adv. Chem. Phys. **56**, 411 (1984).
[34] Z. Chen and R. M. Stratt, J. Chem. Phys. **95**, 2669 (1991).
[35] J. D. Abella, N. A. Kurnit, and S. R. Hartmann, Phys. Rev. A **141**, 391 (1966); T. Mossberg, A. Flusberg, R. Kachru, and S. R. Hartmann, Phys. Rev. Lett. **42**, 1665 (1979).
[36] (a) W. H. Hesselink and D. A. Wiersma, Phys. Rev. Lett. **43**, 1991 (1979); (b) K. Duppen and D. A. Wiersma, J. Opt. Soc. Am. B **3**, 614 (1986); (c) D. A. Wiersma and K. Duppen, Science **237**, 1147 (1987); (d) E. T. J. Nibbering, D. A. Wiersma, and K. Duppen, Phys. Rev. Lett. **66**, 2464 (1991).
[37] P. C. Becker, H. L. Fragnito, J.-Y. Bigot, C. Brito-Cruz, R. L. Fork, and C. V. Shank, Phys. Rev. Lett. **63**, 505 (1989); J.-Y. Bigot, M. T. Portella, R. W. Schoenlein, C. J. Bardeen, A. Migus, and C. V. Shank, *ibid.* **66**, 1138 (1991).
[38] L. E. Fried, N. Bernstein, and S. Mukamel, Phys. Rev. Lett. **68**, 1842 (1992).
[39] N. E. Shemetulskis and R. F. Loring, J. Chem. Phys. **97**, 1217 (1992).
[40] M. Cho and G. R. Fleming, J. Chem. Phys. **98**, 2848 (1993).
[41] A. M. Weiner, S. De Silvestri, and E. P. Ippen, J. Opt. Soc. Am. B **2**, 654 (1985); A. M. Weiner, S. De Silvestri, and E. P. Ippen, in *Ultrafast Phenomena IV*, edited by D. H. Auston and K. B. Eisenthal (Springer, Berlin, 1984), p. 230.
[42] I. Ohmine and H. Tanaka, J. Chem. Phys. **93**, 8138 (1990).
[43] M. Cho, S. Saito, R. M. Stratt, I. Ohmine, and G. R. Fleming (in preparation).
[44] P. Schofield, Phys. Rev. Lett. **4**, 239 (1960).
[45] R. G. Gordon, Adv. Mag. Res. **3**, 1 (1968).


[46] Let $A(t)$ be a quantum mechanical (one-sided) correlation function, $A(t)=\langle Q(0)Q(t)\rangle$. Then, the real $[C(t)]$ and imaginary $[G(t)]$ parts of $A(t)$ are related via the fluctuation-dissipation theorem (Refs. 44 and 45) by

$$G(t)=-\tan\{(\hbar/2k_BT)\partial/\partial t\}C(t) \tag{R1}$$

with

$$A(t)=C(t)-iG(t),$$

$$C(t)\equiv\mathrm{Re}[A(t)]=\tfrac{1}{2}\langle Q(0)Q(t)+Q(t)Q(0)\rangle,$$

$$G(t)\equiv\mathrm{Im}[A(t)]=\tfrac{i}{2}\langle Q(0)Q(t)-Q(t)Q(0)\rangle, \tag{R2}$$

where $k_B$ and $T$ denote the Boltzmann constant and temperature, respectively. $C(t)$ and $G(t)$ are often called the correlation and response (Green, after-effect, or retarded) functions, respectively. Furthermore, defining the Fourier transforms of $C(t)$ and $G(t)$ as

$$C(\omega)\equiv\int_0^\infty dt\, C(t)\cos\omega t \quad\text{and}\quad G(\omega)\equiv\int_0^\infty dt\, G(t)\sin\omega t, \tag{R3}$$

the two spectral densities are connected by

$$G(\omega)=\tanh(\hbar\omega/2k_BT)C(\omega). \tag{R4}$$

In order to obtain Eq. (4.10) we replaced the symmetrized quantum mechanical correlation function with the corresponding classical rotational correlation function $\tilde{\tilde{Y}}_0(t)$ and used the first order expansion term of Eq. (R1).


[47] B. J. Berne and R. Pecora, *Dynamic Light Scattering* (Wiley-Interscience, New York, 1976).
[48] B. J. Berne and G. D. Harp, Adv. Chem. Phys. **17**, 63 (1970).
[49] A. J. Ruggiero, N. F. Scherer, G. M. Mitchell, G. R. Fleming, and J. N. Hogan, J. Opt. Soc. Am. B **8**, 206 (1991).
[50] W. H. Press, B. P. Flannery, S. A. Teukolsky, and W. T. Vetterling, *Numerical Recipes, The Art of Scientific Computing* (Cambridge University, Cambridge, 1986).
[51] A. J. Leggett, S. Chakravarty, A. T. Dorsey, M. P. A. Fisher, A. Garg, and W. Zwerger, Rev. Mod. Phys. **59**, 1 (1987).
[52] W. D. Horrocks and F. A. Cotton, Spectrochim. Acta **17**, 134 (1961).
[53] W. G. Rothschild, *Dynamics of Molecular Liquids* (Wiley-Interscience, New York, 1984).
[54] W. B. Bosma, L. E. Fried, and S. Mukamel, J. Chem. Phys. (in press).
[55] S. Mukamel and Y. J. Yan, Acct. Chem. Res. **22**, 301 (1989).
[56] P. Benassi, V. Mazzacurati, M. Nardone, G. Ruocco, and G. Signorelli, J. Chem. Phys. **91**, 6752 (1989).
[57] A. O. Caldeira and A. J. Leggett, Ann. Phys. **149**, 374 (1983).
[58] R. Zwanzig, Ann. Rev. Phys. Chem. **16**, 67 (1965).
[59] R. Kubo, *Lectures in Theoretical Physics, Vol. I* (Interscience, New York, 1961) pp. 120–203.
[60] R. Zwanzig, J. Stat. Phys. **9**, 215 (1973).
[61] E. Cortes, B. J. West, and K. Lindenberg, J. Chem. Phys. **82**, 2708 (1985).

[62] L. E. Fried and S. Mukamel, Adv. Chem. Phys. (in press).
[63] B. J. Gertner, K. R. Wilson, and J. T. Hynes, J. Chem. Phys. **90**, 3537 (1989).
[64] J. T. Hynes, E. A. Carter, G. Ciccotti, H. J. Kim, D. A. Zichi, M. Ferrario, and R. Kapral, in *Perspectives in Photosynthesis*, edited by J. Jortner and B. Pullman (Kluwer, Dordrecht, 1990), p. 133.
[65] P. Hanggi, P. Talkner, and M. Borkovec, Rev. Mod. Phys. **62**, 251 (1990).
[66] (a) J. S. Bader, R. A. Kuharski, and D. Chandler, J. Chem. Phys. **93**, 230 (1990); (b) D. Chandler, in *Liquids, Freezing, and the Glass Transition, Les Houches, Session LI*, edited by D. Levesque and J. Zinn-Justin (Elsevier, Amsterdam, 1990); (c) J. N. Gehlen and D. Chandler, J. Chem. Phys. **97**, 4958 (1992).
[67] K. Shulten and M. Tesch, Chem. Phys. **158**, 421 (1991).
[68] J. N. Onuchic, D. N. Beratan, and J. J. Hopfield, J. Phys. Chem. **90**, 3706 (1986).
[69] R. D. Coalson, J. Chem. Phys. **94**, 1108 (1991).
[70] Y. Tanimura and S. Mukamel, Phys. Rev. A **47**, 118 (1993).
[71] E. Pollak, J. Chem. Phys. **85**, 865 (1986).
[72] R. F. Grote and J. T. Hynes, J. Chem. Phys. **73**, 2715 (1980).
[73] G. A. Voth, D. Chandler, and W. H. Miller, J. Chem. Phys. **91**, 7749 (1989).
[74] G. Seeley and T. Keyes, in *Spectral Line Shapes*, edited by J. Szudy (Ossolineum, Wroclaw, 1989), Vol. 5, p. 649; G. Seeley and T. Keyes, J. Chem. Phys. **91**, 5581 (1989); B. Madan, T. Keyes, and G. Seeley, *ibid.* **92**, 7565 (1990); **94**, 6762 (1991); G. Seeley, T. Keyes, and B. Madan, *ibid.* **95**, 3847 (1991).
[75] M. Buchner, B. M. Ladanyi, and R. M. Stratt, J. Chem. Phys. **97**, 8522 (1992).